PHYSICAL REVIEW D **95,** 014033 (2017)

Helicity evolution at small x: Flavor singlet and nonsinglet observables

Yuri V. Kovchegov[*]
Department of Physics, The Ohio State University, Columbus, Ohio 43210, USA

Daniel Pitonyak[†]
Division of Science, Penn State University-Berks, Reading, Pennsylvania 19610, USA
and RIKEN BNL Research Center, Brookhaven National Laboratory, Upton, New York 11973, USA

Matthew D. Sievert[‡]
Theoretical Division, Los Alamos National Laboratory, Los Alamos, New Mexico 87545, USA
and Physics Department, Brookhaven National Laboratory, Upton, New York 11973, USA
(Received 1 November 2016; published 30 January 2017)

We extend our earlier results for the quark helicity evolution at small x [J. High Energy Phys. 01 (**2016**) 072] to derive the small-x asymptotics of the flavor singlet and flavor nonsinglet quark helicity TMDs and PDFs and of the g_1 structure function. In the flavor singlet case we rederive the evolution equations obtained in our previous paper on the subject [J. High Energy Phys. 01 (**2016**) 072], performing additional cross-checks of our results. In the flavor nonsinglet case we construct new small-x evolution equations by employing the large-N_c limit. All evolution equations resum double-logarithmic powers of $\alpha_s \ln^2(1/x)$ in the polarization-dependent evolution along with the single-logarithmic powers of $\alpha_s \ln(1/x)$ in the unpolarized evolution which includes saturation effects. We solve the linearized flavor nonsinglet equation analytically, obtaining an intercept which agrees with the one calculated earlier by Bartels, Ermolaev and Ryskin [Z. Phys. C **70**, 273 (1996)] using the infrared evolution equations. Our numerical solution of the linearized large-N_c evolution equations for the flavor singlet case is presented in the accompanying Letter [Phys. Rev. Lett. **118**, 052001 (2017)] and is further discussed here.

DOI: 10.1103/PhysRevD.95.014033

I. INTRODUCTION

Measurements of hadronic structure functions in deep inelastic scattering are kinematically limited to a minimum value of Bjorken-x due to a finite center-of-mass energy $s \propto \frac{1}{x}$. Therefore, all structure functions, and all parton distribution functions (PDF's) $f(x, Q^2)$ extracted from them, must necessarily be extrapolated toward smaller x in order to generate predictions for higher energy scattering experiments and to apply quantum chromodynamics (QCD) sum rules which constrain moments $\int_0^1 dx x^n f(x, Q^2)$ of the PDF's. Structure functions in the $x \to 0$ limit are often singular, with the best-known examples being the unpolarized structure functions F_1 and F_2. At leading twist and leading order in the coupling α_s, F_1 is a weighted measure of the total density of partons in a hadron, with its $x \to 0$ singularity reflecting, in part, the enhancement of soft gluon radiation in QCD. The dynamics of this soft gluon radiation are encapsulated in the Balitsky–Fadin–Kuraev–Lipatov (BFKL) [1,2], Balitsky–Kovchegov (BK) [3–6], and Jalilian-Marian–Iancu–McLerran–Weigert–Leonidov–Kovner (JIMWLK) evolution equations [7–10], which describe the development of a cascade of small-x gluons at high energies by resumming (at leading order) the large logarithms $\alpha_s \ln \frac{s}{\Lambda^2} \sim \alpha_s \ln \frac{1}{x} \sim 1$ (Λ is an infrared cutoff). This parton cascade, as described by the linear BFKL equation, leads to a steep growth in the gluon number density $\frac{dN}{dy} \propto x f(x, Q^2)$ of partons per unit rapidity resulting in a violation of the black disk limit for the corresponding scattering cross sections. This growth is regulated by the onset of the high-density regime of QCD, where nonlinear multiple rescatterings of the parton cascade in the target (as described by the BK and JIMWLK equations) *saturate* the number density of partons such that dN/dy remains finite as $x \to 0$. This results in corresponding cross sections satisfying the black disk limit (see [11–17] for reviews).

The BFKL, BK, and JIMWLK equations, however, cannot describe the small-x limit of the *polarized* structure function g_1, which at leading twist and leading order in α_s is a weighted measure of the quark helicity PDF's $\Delta q^f(x, Q^2)$. The high-energy/small-x asymptotics captured by these evolution equations are insensitive to polarization because, as is well-known, polarization dependence is suppressed at high energies. The subeikonal interactions which do not transfer spin in high-energy scattering enter as power-suppressed corrections to unpolarized cross sections and to F_1 and F_2. The subeikonal interactions which do transfer longitudinal spin provide the *leading* high-energy/small-x asymptotics of the

[*]kovchegov.1@osu.edu
[†]dap67@psu.edu
[‡]sievertmd@lanl.gov

longitudinal double-spin asymmetry A_{LL} and the polarized structure function g_1. The development of a cascade of *polarized* partons at small x is thus an interesting and important aspect of high-energy dynamics in QCD which is outside the scope of the canonical small-x treatment.

The small-x asymptotics of the polarized g_1 structure function were studied previously by Bartels, Ermolaev, and Ryskin (BER) in the flavor singlet [18] and nonsinglet [19] cases. Unlike with unpolarized small-x evolution, in helicity evolution, t-channel quarks play an important role already at the leading order. In the massless limit, quarks automatically transfer spin through the t-channel due to helicity conservation for massless fermions. The effective particle exchanged by such dressed quarks is known as the Reggeon in the small-x literature [20–24], and it has been studied previously in the context of baryon stopping in heavy-ion collisions [25]. In addition to quarks, a power-suppressed component of gluon exchange can also carry spin through the t-channel. While the unpolarized BFKL/BK/JIMWLK evolution occurs through the exchange of dressed, longitudinally polarized gluons (the "hard QCD Pomeron"), helicity evolution receives contributions from exchanging a pair of dressed gluons with one polarized longitudinally and the other transversely [18,19]. The exchange of quarks and of polarized gluons both enter at the same parametric order and can therefore mix with each other, akin to the mixing which occurs in polarized and unpolarized Dokshitzer–Gribov–Lipatov–Altarelli–Parisi (DGLAP) evolution in Q^2 [26–28].

Helicity evolution (like Reggeon evolution) is double-logarithmic, resumming two logarithms of the energy for each power of the coupling: $\alpha_s \ln^2 \frac{s}{\Lambda^2} \sim \alpha_s \ln^2 \frac{1}{x} \sim 1$. In this sense, helicity evolution can be said to be *stronger* than the single-logarithmic BFKL/BK/JIMWLK evolution, leading to the possibility that the helicity PDF's could become (almost) competitive with the unpolarized ones at small x, despite their suppression in the initial conditions. Indeed, this is what BER found [18]: for the flavor singlet case with $N_f = 0$ (pure glue) and $\alpha_s(Q^2) = 0.343$ at $Q^2 = 3$ GeV^2, their results required helicity PDF's to grow at small x as $(\frac{1}{x})^{1.481}$. In comparison, leading-order fixed-coupling BFKL evolution with the same parameters yields unpolarized PDF's which grow at small x as $(\frac{1}{x})^{1.908}$. The presence of a nonintegrable singularity in the helicity PDF's would imply that their contribution to the proton spin $S_q = \frac{1}{2}\sum_f \int_0^1 dx \Delta q^f(x, Q^2)$ is not finite, requiring either higher-order corrections or nonlinear saturation effects at small x to regulate the divergence. The latter scenario would potentially provide a novel path to discovering parton saturation using measurements of the polarized structure functions instead of the unpolarized ones.

Motivated by this possibility, and by the need to assess the amount of proton spin at small x, we derived in a previous work [29] evolution equations for the quark helicity PDF's at small x, including the nonlinear multiple rescattering which drives parton saturation. Our approach used the modern saturation formalism, relating the helicity PDF's to a polarized dipole amplitude which we calculated in light-front perturbation theory (LFPT) [30]. The resulting evolution equations involve quark and gluon Wilson line operators, along with an object we refer to as the "polarized Wilson line": an eikonal quark or gluon propagator with the insertion of one or two subeikonal vertices carrying polarization information. These equations do not close in general because they involve higher-order operators in the evolution kernel; this should result in a helicity analogue of the Balitsky hierarchy [3,4]. However, also by analogy to the unpolarized case, our helicity evolution equations do close in the large-N_c and large-N_c & N_f limits, with N_c the number of colors and N_f the number of flavors. The equations are quite complex and difficult to solve, even in the linearized strictly double-logarithmic regime. In an accompanying Letter [31] we present the numerical solution of our equations at large N_c, obtaining the helicity intercept of $\alpha_h \approx 2.31\sqrt{\frac{\alpha_s N_c}{2\pi}}$. This leads to helicity PDF's with *integrable* singularities at small x, scaling as $\Delta q \sim (\frac{1}{x})^{\alpha_h} \sim (\frac{1}{x})^{0.936}$ for $N_f = 0$ and $Q^2 = 3$ GeV^2, and hence a finite value of the quark spin contribution S_q. Such a scenario would not, in fact, require saturation effects to regulate the small-x limit after all.

Somewhat surprisingly, the value of our helicity intercept in the flavor singlet channel is smaller than that obtained by BER by about 35% [18]. To understand the source of our significant discrepancy with BER, we have performed a variety of consistency checks of our equations, which we present here in detail. This analysis also sheds further light on the intricate structure of helicity evolution at small x, which is substantially more complex than the unpolarized evolution which is well-known in the literature.

While our previous paper [29] dealt with flavor-singlet helicity observables, here we have also generalized the treatment to include flavor nonsinglet helicity PDF's and transverse momentum-dependent PDF's (TMD's), along with the g_1 structure function. Constructing a large-N_c helicity evolution equation for the flavor nonsinglet case, we have reproduced the flavor nonsinglet intercept obtained previously by BER [19].

This paper is organized as follows. In Sec. II we rederive, cross-check and present a solution for the helicity evolution equations in the flavor singlet case derived previously in [29]. We relate the polarized flavor-singlet observables to a "polarized dipole amplitude" which contains the dynamics of spin exchange at small x in Sec. II A, and we state our initial conditions for this amplitude. The large-N_c flavor-singlet helicity evolution equations are presented in Sec. II B; they are solved numerically in the accompanying Letter [31]. We discuss the solution in Sec. II C and outline our disagreement with BER. In Sec. II D we perform a number of explicit calculations which elucidate the role of virtual corrections in our evolution equations and which verify the real-virtual

cancellations used in deriving them. In Sec. II E we use our evolution equations to compute the glue/glue next-to-leading order (NLO) anomalous dimension in polarized DGLAP evolution, again obtaining agreement with the literature [32] and with BER on this point. The flavor nonsinglet evolution is constructed in Sec. III, following the same pattern. The flavor nonsinglet observables are defined in Sec. III A in terms of the flavor nonsinglet "polarized dipole amplitude". The helicity evolution equations in the flavor nonsinglet case and in the large-N_c limit are derived in Sec. III B, and are solved analytically in Sec. III C, leading to an intercept in perfect agreement with [19]. In Sec. IV we conclude by summarizing the importance of our calculation for assessing the small-x contribution to the spin puzzle.

II. FLAVOR SINGLET HELICITY EVOLUTION

A. Definitions and initial conditions

As was derived in [29,33], at small x, the polarized structure function $g_1(x,Q^2)$, the quark helicity PDF $\Delta q(x,Q^2)$, and the quark helicity TMD $g_{1L}(x,k_T^2)$ can all be expressed in the following way:

$$g_1(x,Q^2) = \frac{N_c}{(2\pi)^2\alpha_{\rm EM}}\int_{z_i}^1 \frac{dz}{z^2(1-z)}\int dx_{01}^2 d^2b\left[\frac{1}{2}\sum_{\lambda\sigma\sigma'}|\psi^T_{\lambda\sigma\sigma'}|^2_{(x_{01}^2,z)} + \sum_{\sigma\sigma'}|\psi^L_{\sigma\sigma'}|^2_{(x_{01}^2,z)}\right] \times \frac{1}{2N_c}\left\{\langle\!\langle {\rm tr}[V_{\underline{0}}V_{\underline{1}}^{\rm pol\dagger}]\rangle\!\rangle(z) + \langle\!\langle {\rm tr}[V_{\underline{0}}V_{\underline{1}}^{\rm pol\dagger}]\rangle\!\rangle^*(z)\right\}, \tag{1a}$$

$$\Delta q(x,Q^2) = \frac{N_c}{4\pi^3}\int_{z_i}^1\frac{dz}{z}\int_{\frac{1}{zs}}^{\frac{1}{zQ^2}}\frac{dx_{01}^2}{x_{01}^2}\int d^2b\,\frac{1}{2N_c}\{\langle\!\langle {\rm tr}[V_{\underline{0}}V_{\underline{1}}^{\rm pol\dagger}]\rangle\!\rangle(z) + \langle\!\langle {\rm tr}[V_{\underline{0}}V_{\underline{1}}^{\rm pol\dagger}]\rangle\!\rangle^*(z)\}, \tag{1b}$$

$$g_{1L}(x,k_T^2) = \frac{4N_c}{(2\pi)^6}\int_{z_i}^1\frac{dz}{z}\int d^2x_{01}d^2x_{0'1}e^{-i\underline{k}\cdot(\underline{x}_{01}-\underline{x}_{0'1})}\frac{\underline{x}_{01}\cdot\underline{x}_{0'1}}{x_{01}^2x_{0'1}^2} \times\int d^2b\,\frac{1}{2N_c}\{\langle\!\langle {\rm tr}[V_{\underline{0}}V_{\underline{1}}^{\rm pol\dagger}]\rangle\!\rangle(z) + \langle\!\langle {\rm tr}[V_{\underline{0}}V_{\underline{1}}^{\rm pol\dagger}]\rangle\!\rangle^*(z)\}. \tag{1c}$$

These results come from the computation of the diagrams shown in Fig. 1 in LFPT in the conventions of [17], where we take the virtual photon with virtuality Q^2 to have a large momentum along the light-front "+" axis and work in the $A^+=0$ gauge. The diagrams in Fig. 1 represent contributions to the polarization-dependent part of the quark production cross section in semi-inclusive deep inelastic scattering (SIDIS) on a polarized target proton or nucleus; the quark helicity TMD and PDF and the g_1 structure function can be extracted from this quantity [29]. The notation is defined as in Fig. 1: σ,σ',λ are the polarizations of the quark, antiquark, and (transverse) photon, respectively (we take the target to have positive helicity, without loss of generality); $\underline{x}_1$ is the transverse coordinate of the antiquark which scatters in a polarization-dependent way; $\underline{x}_0$ and $\underline{x}_{0'}$ are the transverse coordinates of the produced quark in the amplitude and complex-conjugate amplitude, respectively; and z is the fraction of the photon's "+" momentum which is carried by the antiquark. Transverse vectors are denoted $\underline{v}\equiv(v_\perp^1,v_\perp^2)$, with $v_\perp = v_T \equiv |\underline{v}|$, and the separation vector between coordinates is $\underline{x}_{ij}\equiv\underline{x}_i-\underline{x}_j$. The dipole impact parameter is defined by $\underline{b}=(\underline{x}_1+\underline{x}_0)/2$. The z integral has a lower cutoff $z_i = \Lambda^2/s$ with Λ the infrared (IR) cutoff and s the center-of-mass energy squared for the SIDIS process pictured in Fig. 1. N_c is the number of colors and $\alpha_{\rm EM}$ is the fine structure constant. The light cone wave functions for the $\gamma^*\to q\bar{q}$ splitting are denoted $\psi^T_{\lambda\sigma\sigma'}$ and $\psi^L_{\sigma\sigma'}$ for the

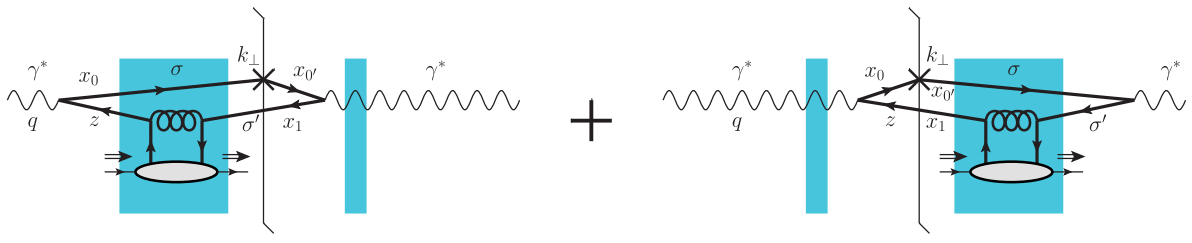

FIG. 1. Diagrams contributing to the quark helicity at small-x. The shaded region is the shock wave of the (polarized) target. The spin-dependent interaction is illustrated by t-channel quark exchanges, but in general should include gluon exchanges as well (see text).

transverse and longitudinal polarizations of the virtual photon respectively. These functions are well-known in the literature [34,35], and are explicitly given e.g. in [29].

In obtaining the simplified expressions (1) we have taken the produced quarks to be massless and utilized parity symmetry of the virtual photon wave functions. In arriving at Eq. (1c) we have used the $\underline{k} \to -\underline{k}$ symmetry of the helicity TMD due to the absence of any preferred transverse direction in the problem [29]. The parton distribution functions in Eqs. (1) are given to leading-twist accuracy, and the structure function g_1 is given in the double-logarithmic approximation. Note that so far we assume that only one (massless) quark flavor enters the loop in the diagrams of Fig. 1.

The fundamental-representation Wilson line $V_{\underline{0}}$ in Eqs. (1) is the usual path-ordered exponential which describes the gauge rotation of an eikonal quark passing through a background gluon field of the target proton or nucleus:

$$V_{\underline{x}} \equiv \mathcal{P} \exp\left[ig \int_{-\infty}^{\infty} dx^+ A^-(x^+, 0^-, \underline{x})\right]. \tag{2}$$

Note the abbreviated notation $V_{\underline{0}} \equiv V_{\underline{x}_0}$.

The "polarized Wilson lines" $V_{\underline{x}}^{\rm pol}$ are more difficult to define operatorially. Consider an eikonal quark propagator with the insertion of either one (for gluon exchange) or two (for quark exchange) subeikonal polarization-dependent vertices. The resulting propagator of an eikonal quark with polarization σ in the background quark or gluon field of the target is written as

$$V_{\underline{x}}(\sigma) \equiv V_{\underline{x}} + \sigma V_{\underline{x}}^{\rm pol} \tag{3}$$

with the polarization-dependent part of that background-field propagator being more than a pure gauge rotation. The polarized Wilson line may couple once to a transverse component $A_\perp^i$ of the gluon field, or it may exchange two t-channel quarks with the target. Since the leading high-energy behavior of the quark propagator is spin-independent, $V_{\underline{x}}^{\rm pol}$ is suppressed relative to $V_{\underline{x}}$ by a factor of the quark energy. Each additional spin-dependent interaction is further suppressed by a power of the quark energy, so $V_{\underline{x}}^{\rm pol}$ contains exactly one spin-dependent interaction (a gluon exchange or a two-quark exchange), along with any number of eikonal, spin-independent gluon-exchange interactions. The double angle brackets in (9b) are defined to remove this suppression of $1/zs$ from the dipole trace [29],

$$\langle\!\langle \mathcal{O} \rangle\!\rangle(z) \equiv zs \langle \mathcal{O} \rangle(z), \tag{4}$$

while the single angle brackets $\langle \ldots \rangle$ denote the averaging in the (polarized) target proton or nucleus. Note that z used in the rescaling is the momentum fraction of the polarized line in the dipole, while z in the argument is the smallest momentum fraction between the polarized and unpolarized lines [29]: these two z values could be different.

To further simplify Eqs. (1) it would be tempting to replace

$$\langle\!\langle {\rm tr}[V_{\underline{0}} V_{\underline{1}}^{\rm pol\dagger}] \rangle\!\rangle^*(z) \to \langle\!\langle {\rm tr}[V_{\underline{1}}^{\rm pol} V_{\underline{0}}^\dagger] \rangle\!\rangle(z) \tag{5}$$

as is often done for the unpolarized small-x evolution (the asterisk denotes complex conjugation). However, here one has to be more careful: for a general target state $|T\rangle$ we have

$$\langle T|{\rm tr}[V_{\underline{0}} V_{\underline{1}}^{\rm pol\dagger}]|T\rangle^* = \langle \overline{T}|{\rm tr}[V_{\underline{1}}^{\rm pol} V_{\underline{0}}^\dagger]|\overline{T}\rangle, \tag{6}$$

where $|\overline{T}\rangle$ denotes the charge-conjugate target state. While unpolarized BFKL, BK and JIMWLK evolution is insensitive to whether the target is, say, a quark or an antiquark, this is not the case for helicity evolution. For instance, the t-channel quark exchange shown in Fig. 1 is possible for the quark target but is impossible for the antiquark one.

Keeping this in mind, let us consider the flavor singlet case,

$$\Delta q^S(x, Q^2) \equiv \sum_f [\Delta q^f(x, Q^2) + \Delta \overline{q}^f(x, Q^2)]. \tag{7}$$

Adding to diagrams in Fig. 1 the graphs which have the quark loop particle number flow in the opposite direction (such that the tagged particle is an antiquark) and summing over all flavors simplifies Eqs. (1) to

$$g_1^S(x, Q^2) = \frac{N_c}{2\pi^2 \alpha_{\rm EM}} \sum_f \int_{z_i}^1 \frac{dz}{z^2(1-z)} \times \int dx_{01}^2 \left[\frac{1}{2} \sum_{\lambda\sigma\sigma'} |\psi^T_{\lambda\sigma\sigma'}|^2_{(x_{01}^2, z)} + \sum_{\sigma\sigma'} |\psi^L_{\sigma\sigma'}|^2_{(x_{01}^2, z)}\right] G(x_{01}^2, z), \tag{8a}$$

$$\Delta q^S(x, Q^2) = \frac{N_c}{2\pi^3} \sum_f \int_{z_i}^1 \frac{dz}{z} \int_{\frac{1}{zs}}^{\frac{1}{zQ^2}} \frac{dx_{01}^2}{x_{01}^2} G(x_{01}^2, z), \tag{8b}$$

$$g_{1L}^S(x, k_T^2) = \frac{8N_c}{(2\pi)^6} \sum_f \int_{z_i}^1 \frac{dz}{z} \int d^2x_{01} d^2x_{0'1} \times e^{-i\underline{k}\cdot(\underline{x}_{01} - \underline{x}_{0'1})} \frac{\underline{x}_{01} \cdot \underline{x}_{0'1}}{x_{01}^2 x_{0'1}^2} G(x_{01}^2, z). \tag{8c}$$

We see from Eqs. (8) that the small-x polarized scattering dynamics are contained within the *polarized* dipole *amplitude*, which is defined by

$$G_{10}(z) \equiv \frac{1}{2N_c} \langle\!\langle {\rm tr}[V_{\underline{0}} V_{\underline{1}}^{\rm pol\dagger}] + {\rm tr}[V_{\underline{1}}^{\rm pol} V_{\underline{0}}^\dagger] \rangle\!\rangle(z) = G(\underline{x}_1, \underline{x}_0, z) = G(\underline{x}_{10}, \underline{b}, z), \tag{9a}$$

$$G(x_{01}^2, z) \equiv \int d^2b G_{10}(z), \tag{9b}$$

where, again, $\underline{b} = \frac{1}{2}(\underline{x}_1 + \underline{x}_0)$ is the impact parameter of the dipole which is held fixed in $G_{10}(z)$ and integrated in

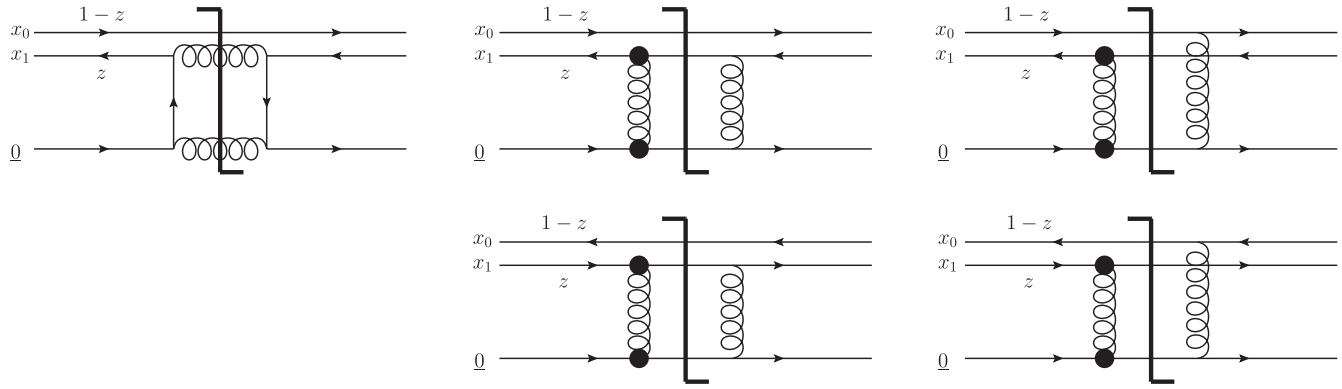

FIG. 2. Diagrams contributing to the lowest-order initial conditions $G_{01}^{(0)}(z)$ for a quark target. The top line of diagrams contributes to $\mathrm{tr}[V_0 V_1^{\mathrm{pol}\dagger}]$, and the bottom line contributes to $\mathrm{tr}[V_1^{\mathrm{pol}} V_0^\dagger]$. The black circles denote noneikonal quark-gluon vertices which transfer spin, and complex-conjugates must be added to the asymmetric diagrams. Note that in the second line, the quark and antiquark lines have been interchanged, consistent with the definition (9a).

$G(x_{01}^2, z)$. In arriving at Eqs. (9) we have assumed that $G_{10}(z)$ and, hence, $G(x_{01}^2, z)$ are both real, $G_{10}(z) = G_{10}^*(z)$, which is true for the leading contributions to $G_{10}(z)$ without evolution (the initial conditions) and is still the case after evolving the polarized dipole amplitude using helicity evolution [29]. The helicity evolution equations constructed in [29] concentrated on the flavor singlet case of Eqs. (8) and (9).

Although the polarized Wilson line defining $G_{10}(z)$ is difficult to define operatorially, it corresponds to the spin-dependent part of the S-matrix of a quark propagating through the background field of the target. Therefore, we can define $G_{10}(z)$ indirectly by relating it to the dipole cross section via the optical theorem,

$$\begin{aligned}\frac{1}{N_c}\langle \mathrm{tr}[V_{\underline{0}}(\sigma_0) V_{\underline{1}}^\dagger(\sigma_1)]\rangle(z) &\equiv S[q_{\underline{0}}(\sigma_0), \overline{q}_{\underline{1}}(\sigma_1), zs] \\ &\approx 1 - \mathrm{Im}T[q_{\underline{0}}(\sigma_0), \overline{q}_{\underline{1}}(\sigma_1), zs] \\ &= 1 - \frac{1}{2}\frac{d\sigma}{d^2b}[q_{\underline{0}}(\sigma_0), \overline{q}_{\underline{1}}(\sigma_1), zs],\end{aligned} \tag{10}$$

where we have neglected the real part of the (expectation value of the) T-matrix at high energies as being higher-order in the strong coupling α_s.[1] Here $q_{\underline{x}}(\sigma)$ $(\overline{q}_{\underline{x}}(\sigma))$ denotes a quark (antiquark) at transverse position $\underline{x}$ and spin σ. Using (3) to expand the Wilson lines on the left-hand side, we obtain

$$\begin{aligned}\frac{1}{N_c}\langle \mathrm{tr}[V_{\underline{0}} V_{\underline{1}}^{\mathrm{pol}\dagger}]\rangle(z) &= -\frac{1}{4}\sum_{\sigma_0\sigma_1}\sigma_1 \frac{d\sigma}{d^2b}[q_{\underline{0}}(\sigma_0), \overline{q}_{\underline{1}}(\sigma_1), zs] \\ &\equiv -\frac{d\sigma}{d^2b}[q_{\underline{0}}^{unp}, \Delta\overline{q}_{\underline{1}}, zs],\end{aligned} \tag{11}$$

and similarly for $\frac{1}{N_c}\langle \mathrm{tr}[V_{\underline{1}}^{\mathrm{pol}} V_{\underline{0}}^\dagger]\rangle(z)$. This gives an expression for the polarized dipole amplitude in terms of the spin-dependent part of the dipole cross section,

$$G_{10}(z) = -\frac{zs}{2}\left(\frac{d\sigma}{d^2b}[q_{\underline{0}}^{unp}, \Delta\overline{q}_{\underline{1}}, zs] + \frac{d\sigma}{d^2b}[\overline{q}_{\underline{0}}^{unp}, \Delta q_{\underline{1}}, zs]\right). \tag{12}$$

With the help of (12), we can calculate the polarized dipole amplitude at lowest order for a quark target as shown in Fig. 2. For simplicity the target quark is assumed to be at the origin in the transverse plane. These explicit expressions for $G_{10}^{(0)}$ can serve as initial conditions for the subsequent small-x evolution,

$$G_{10}^{(0)} = \frac{\alpha_s^2 C_F}{N_c}\left[\frac{C_F}{x_1^2} - 2\pi\delta^2(\underline{x}_1)\ln(zsx_{10}^2)\right] \tag{13a}$$

$$G^{(0)}(x_{10}^2, z) = \frac{\alpha_s^2 C_F}{N_c}\pi\left[C_F \ln\frac{zs}{\Lambda^2} - 2\ln(zsx_{10}^2)\right], \tag{13b}$$

where the impact parameter integral $\int d^2b = \int d^2x_0 = \int d^2x_1$ is cut off in the UV by the energy $b^2 > \frac{1}{zs}$ and in the IR by a cutoff $b^2 < \frac{1}{\Lambda^2}$, while $C_F = (N_c^2 - 1)/2N_c$. One can also dress these linearized expressions with quasiclassical multiple Glauber-Mueller (GM) rescatterings [38] in the spirit of the McLerran-Venugopalan (MV) model [39–44], obtaining

[1]There is a subtlety here: the real part of the unpolarized T-matrix for eikonal Wilson lines, the odderon [36,37], is α_s-suppressed compared to the leading unpolarized imaginary part retained in Eq. (10). In our power counting, this makes the unpolarized real part much larger than the leading polarization-dependent imaginary part we are interested in, since the latter is energy-suppressed. Hence, the approximation in Eq. (10) should be understood as correctly retaining only the leading polarized and unpolarized contributions.

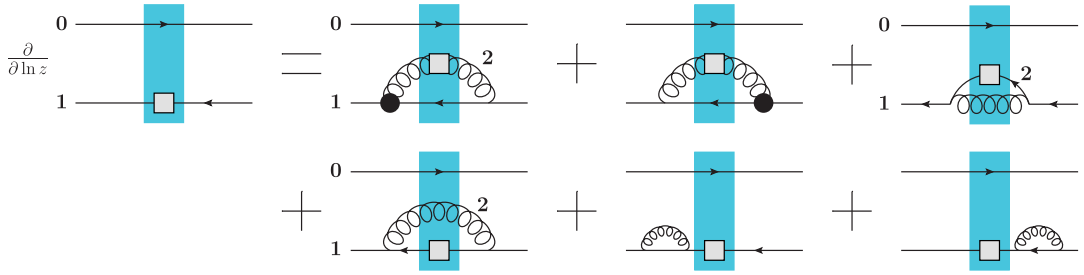

FIG. 3. One step of small-x evolution in the polarized dipole amplitude G_{10}. The thick vertical rectangle represents the shock wave interaction with the target, the large black circle vertices represent the subeikonal emission of a polarized gluon, and the small gray box denotes the polarized Wilson line. For simplicity, the initial condition $G_{10}^{(0)}$ is not shown.

$$G_{10}^{(0)} = \frac{\alpha_s^2 C_F}{N_c}\left[\frac{C_F}{x_1^2} - 2\pi\delta^2(\underline{x}_1)\ln(zsx_{10}^2)\right] \times \exp\left[-\frac{1}{4}x_{10}^2 Q_s^2(b)\ln\frac{1}{x_{01}\Lambda}\right] \tag{14}$$

where Q_s is the saturation scale before evolution. Equation (14) includes saturation effects by resumming multiple rescatterings and can also serve as the initial condition for small-x helicity evolution, if the latter includes saturation effects as well.

B. Flavor singlet helicity evolution at small x

As derived in [29], the small-x evolution of the polarized dipole amplitude resums double logarithms of the energy: $\alpha_s \ln^2 \frac{s}{\Lambda^2} \sim \alpha_s \ln^2 \frac{1}{x}$. The polarized evolution proceeds by the radiation of longitudinally soft polarized partons with momentum fractions $z' \ll z$ (top line of Fig. 3); there are also nonvanishing double-logarithmic contributions from the radiation of longitudinally soft *unpolarized* gluons akin to the unpolarized BFKL/BK/JIMWLK equations (bottom line of Fig. 3). The contribution of other polarized and unpolarized gluon emission diagrams amounts to introducing an IR cutoff $x_{21} < x_{10}$ on the x_{21}-integral in the gluon-emission diagrams in Fig. 3 [29]: for brevity we do not show those remaining graphs. The result of one step of double-logarithmic (DLA) evolution in the polarized dipole amplitude is given by [29]

$$\begin{aligned} G_{10}(z) = G_{10}^{(0)}(z) + \frac{\alpha_s}{2\pi^2}\int_{\Lambda^2/s}^{z}\frac{dz'}{z'}\int\frac{d^2x_2}{x_{21}^2}\theta\left(x_{21}^2 - \frac{1}{z's}\right) \\ \times\Big\{\theta(x_{10}-x_{21})\frac{1}{N_c}\langle\!\langle \mathrm{tr}[t^b V_{\underline{0}} t^a V_{\underline{1}}^\dagger](U_{\underline{2}}^{\mathrm{pol}})^{ba} + \mathrm{tr}[t^b V_{\underline{1}} t^a V_{\underline{0}}^\dagger](U_{\underline{2}}^{\mathrm{pol}\dagger})^{ab}\rangle\!\rangle(z') \\ + \theta(x_{10}^2 z - x_{21}^2 z')\frac{1}{4N_c}[\langle\!\langle \mathrm{tr}[V_{\underline{0}}V_{\underline{1}}^\dagger]\mathrm{tr}[V_{\underline{1}}V_{\underline{2}}^{\mathrm{pol}\dagger}] + \mathrm{tr}[V_{\underline{1}}V_{\underline{0}}^\dagger]\mathrm{tr}[V_{\underline{2}}^{\mathrm{pol}}V_{\underline{1}}^\dagger]\rangle\!\rangle(z') \\ - \frac{1}{2N_c}\langle\!\langle \mathrm{tr}[V_{\underline{0}}V_{\underline{2}}^{\mathrm{pol}\dagger}] + \mathrm{tr}[V_{\underline{2}}^{\mathrm{pol}}V_{\underline{0}}^\dagger]\rangle\!\rangle(z')] \\ + \theta(x_{10}-x_{21})\frac{1}{N_c}[\langle\!\langle \mathrm{tr}[V_{\underline{0}}V_{\underline{2}}^\dagger]\mathrm{tr}[V_{\underline{2}}V_{\underline{1}}^{\mathrm{pol}\dagger}] + \mathrm{tr}[V_{\underline{2}}V_{\underline{0}}^\dagger]\mathrm{tr}[V_{\underline{1}}^{\mathrm{pol}}V_{\underline{2}}^\dagger]\rangle\!\rangle(z') \\ - N_c\langle\!\langle \mathrm{tr}[V_{\underline{0}}V_{\underline{1}}^{\mathrm{pol}\dagger}] + \mathrm{tr}[V_{\underline{1}}^{\mathrm{pol}}V_{\underline{0}}^\dagger]\rangle\!\rangle(z')]\Big\} \end{aligned} \tag{15}$$

as drawn diagrammatically in Fig. 3. The polarized adjoint Wilson line $U_{\underline{2}}^{\mathrm{pol}}$ is defined analogously to (3). Like equations in the Balitsky hierarchy [3,4] for unpolarized small-x evolution, the evolution of the polarized dipole G_{10} is not closed, coupling to increasingly complex operators at each step of evolution. The first term in braces in (15) corresponds to the radiation of a soft polarized gluon, as shown in the first two diagrams of Fig. 3. The second term corresponds to the radiation of a soft polarized (anti)quark, as shown in the third diagram of Fig. 3. The last term in braces in (15) corresponds to the radiation of soft unpolarized gluons, as shown in the second row of diagrams in Fig. 3. As we have already mentioned, the diagrams in the first and third classes are DLA in the $x_{21} < x_{10}$ portion of the full phase space $x_{10}^2 z \gg x_{21}^2 z'$ due to partial cancellations from other diagrams which we do not show explicitly.

Equation (15) does not close, and represents the lowest-order equation in the infinite tower of equations involving higher and higher order operators (in the number of Wilson lines), the helicity evolution analogue of the unpolarized Balitsky hierarchy [3]. This helicity hierarchy, represented here by the evolution equation (15), is difficult to solve; at the moment it is too early to tell whether it would be suitable for stochastic methods used in solving the unpolarized JIMWLK evolution [45]. It can, however, be solved in limits in which the operator hierarchy closes: namely the large-N_c limit and the large-N_c & N_f limit [29]. In the large-N_c limit the evolution is gluon-driven (cf. [46–48]). Assuming that the parent dipole 10 in Fig. 3 comes from the quark and antiquark lines of different gluons at large N_c, we can neglect the radiation of soft quarks [second term in braces in (15)] and simplify the remaining terms, obtaining [29]

$$G_{10}(z) = G_{10}^{(0)}(z) + \frac{\alpha_s N_c}{2\pi^2}\int_{\Lambda^2/s}^{z}\frac{dz'}{z'} \times \int \frac{d^2x_2}{x_{21}^2}\theta(x_{10}-x_{21})\theta\left(x_{21}^2-\frac{1}{z's}\right) \times [2\Gamma_{20,21}(z')S_{21}(z') + 2G_{21}(z')S_{02}(z') + G_{12}(z')S_{02}(z') - \Gamma_{10,21}(z')] \tag{16a}$$

$$\Gamma_{20,21}(z') = G_{20}^{(0)}(z') + \frac{\alpha_s N_c}{2\pi^2}\int_{\Lambda^2/s}^{z'}\frac{dz''}{z''} \times \int \frac{d^2x_3}{x_{32}^2}\theta\left(\min\left[x_{02}^2, x_{21}^2\frac{z'}{z''}\right]-x_{32}^2\right)\theta\left(x_{32}^2-\frac{1}{z''s}\right) \times [2\Gamma_{30,32}(z'')S_{23}(z'') + 2G_{32}(z'')S_{03}(z'') + G_{23}(z'')S_{03}(z'') - \Gamma_{20,32}(z'')], \tag{16b}$$

where the unpolarized dipole scattering amplitude

$$S_{21}(z) \equiv \frac{1}{N_c}\langle \mathrm{tr}[V_{\underline{2}}V_{\underline{1}}^{\dagger}]\rangle \approx S_{12}(z) \tag{17}$$

is obtained from the BK/JIMWLK evolution equations [3–10] with the initial condition given by the GM/MV result [38,49]

$$S_{10}^{(0)}(z) = \exp\left[-\frac{1}{4}x_{10}^2 Q_s^2(\underline{b})\ln\frac{1}{x_{10}\Lambda}\right] \tag{18}$$

which is independent of z. Since BK and JIMWLK evolution is leading-logarithmic (LLA) at the leading order, it does not contribute in the strict DLA limit, in which we simply put $S = 1$ in Eqs. (16). However, when the precision of helicity evolution is increased beyond DLA to LLA level, saturation effects would come in through $S_{21}(z)$ as shown in Eqs. (16).

Even in the large-N_c limit, the operator evolution (15) remains a system of equations because the dipoles are not all independent of each other. The general phase space which yields DLA contributions

$$z_1 x_{1T}^2 \gg z_2 x_{2T}^2 \gg z_3 x_{3T}^2 \cdots \qquad 1 \gg z_1 \gg z_2 \gg z_3 \cdots \tag{19}$$

competes with the $\theta(x_{10}-x_{21})$ functions of (15) which arise from partial cancellations with other diagrams. In some cases, the ordering (19) is more restrictive than the θ functions, which introduces an extra dependence of one dipole amplitude on the dipole size of another. This leads to the "neighbor dipole" function $\Gamma_{20,21}(z')$ [29]. [Note: the labeling here is different than in [29]. Here the first index of Γ denotes the polarized line, bringing it into consistency with G_{10} defined in (9a).] In this term, further evolution continues in the large dipole x_{20}^2, but residual dependence on the size of the neighbor dipole x_{21}^2 remains through the limits of integration in (16b). Thus even in the large-N_c limit, helicity evolution is, in this respect, more complex than unpolarized evolution. We note that the virtual corrections (last term in brackets) can be shown to enter as neighbor dipole functions (see Sec. II D).

There is another interesting feature in the Eqs. (16). Let us first note that the small-x polarized leading-order DGLAP splitting functions for gluon emission are $\Delta P_{Gq}(z\to 0) = 2C_F(\alpha_s/2\pi)$ and $\Delta P_{GG}(z\to 0) = 4N_c(\alpha_s/2\pi)$ [28]. Hence, in the large-N_c limit we have $\Delta P_{GG}(z\to 0) = 4\Delta P_{Gq}(z\to 0)$. The difference between the two splitting functions is not simply due to the difference of their color factors, $C_F \approx N_c/2$ and N_c respectively, as is the case for the unpolarized small-x splitting functions [for which $P_{GG}(z\to 0) = 2P_{Gq}(z\to 0)$]: this would only account for a factor of 2 difference. The other factor of 2 comes from the helicity dynamics of the $G\to GG$ splitting as compared to the $q\to Gq$ splitting. Thus, for the large-N_c limit, which is dominated by gluon dynamics, it is insufficient to simply take Eq. (15) and send $N_c\to\infty$. There is an essential difference between the evolution of the polarized quark dipole and the polarized dipole made out of "quark lines" in the large-N_c gluon dipole: the splitting in the latter come with an extra factor of 2. This is the reason for the extra factor of 2 in front of the first two terms in the integrands of both Eqs. (16). In the large-N_c limit one should understand the polarized dipole definition (9a) as involving eikonal quark and antiquark lines coming from gluon lines. To derive this factor of 2 more formally one needs to start with the analogue of Eq. (15) for the polarized gluon dipole and take the large-N_c limit: this is presented in Appendix A.

C. Solution of flavor singlet helicity evolution equations at large N_c

To facilitate solving the large-N_c equations (16), let us first linearize them by dropping the unpolarized multiple

rescattering terms like S_{21} and then integrate over the impact parameter $\underline{b}$. This is justified outside of the saturation region, where $S \approx 1$. Note also that the S-terms are LLA and should be put to one in the strict DLA limit. Doing so, we obtain

$$G(x_{10}^2, z) = G^{(0)}(x_{10}^2, z) + \frac{\alpha_s N_c}{2\pi} \int_{\frac{1}{x_{10}^2 s}}^{z} \frac{dz'}{z'} \int_{\frac{1}{z's}}^{x_{10}^2} \frac{dx_{21}^2}{x_{21}^2} [\Gamma(x_{10}^2, x_{21}^2, z') + 3G(x_{21}^2, z')], \tag{20a}$$

$$\Gamma(x_{10}^2, x_{21}^2, z') = G^{(0)}(x_{10}^2, z') + \frac{\alpha_s N_c}{2\pi} \int_{\frac{1}{x_{10}^2 s}}^{z'} \frac{dz''}{z''} \int_{\frac{1}{z''s}}^{\min\left[x_{10}^2, x_{21}^2 \frac{z'}{z''}\right]} \frac{dx_{32}^2}{x_{32}^2} \times [\Gamma(x_{10}^2, x_{32}^2, z'') + 3G(x_{32}^2, z'')], \tag{20b}$$

where we have neglected the small differences between the large dipole sizes $x_{01}^2 \approx x_{02}^2 \approx x_{03}^2$.

The usual Laplace-Mellin transform technique fails to simplify the system (20) due to the presence of the neighbor dipole function $\Gamma(x_{10}^2, x_{21}^2, z')$. Instead we resort to solving (20) numerically by discretizing the independent variables on a lattice. Since the z, z' dependence enters through the upper limits of the z', z'' integrations, respectively, these equations are well-suited to solution by iteration: starting with just the initial conditions at $z = \frac{1}{x_{10}^2 s}$, we can systematically compute the polarized dipole amplitude at z using the already-tabulated results for lower values of z. By evolving to sufficiently large zs, we look for the emergence of power-law behavior $G(x_T^2, zs) \propto (zs)^{\alpha_h}$ and extract the helicity intercept α_h by performing a linear fit to $\ln G$. For further details of the numerics and for the implications regarding the quark contribution S_q to the proton spin, we refer the interested reader to the accompanying Letter [31].

The high-energy asymptotics of the polarized dipole amplitude found in [31] can be summarized by

$$G(x_{10}^2, z) \propto (zs)^{\alpha_h} \quad \text{with} \quad \alpha_h \approx 2.31 \sqrt{\frac{\alpha_s N_c}{2\pi}}. \tag{21}$$

Using Eqs. (8) we conclude that the small-x asymptotics of flavor-singlet helicity observables is

$$g_1^S(x, Q^2) \sim \Delta q^S(x, Q^2) \sim g_{1L}^S(x, k_T^2) \sim \left(\frac{1}{x}\right)^{\alpha_h} \approx \left(\frac{1}{x}\right)^{2.31\sqrt{\frac{\alpha_s N_c}{2\pi}}}. \tag{22}$$

This is one of the main results of this project so far.

Our evolution equations (15) only close in the large-N_c or large-N_c & N_f limits. In [31] we have only solved them numerically in the large-N_c (pure glue) limit obtaining the result given in Eq. (21). Solution of the evolution equations derived in [29] for the large-N_c & N_f limit is left for future work.

The intercept in Eq. (21) is smaller by about 35% than the pure glue intercept obtained by BER in [18], $\alpha_h^{\text{BER}} = 3.66\sqrt{\frac{\alpha_s N_c}{2\pi}}$. Despite this disagreement on the full result,[2] we agree with BER on important subsets of the calculation such as the "ladder graphs" which include DGLAP-like quark/gluon mixing [29] and the flavor non-singlet helicity evolution intercept which we obtain below in Eq. (66).

Given this discrepancy, it is important to validate the internal consistency of our calculation and to compare with the results of BER wherever possible. Direct comparison is difficult on a term-by-term or diagram-by-diagram basis, since we work in different gauges (the light cone gauge versus Feynman gauge) and use very different formalisms (s-channel light-front wave functions versus infrared evolution equations). There are, however, some consistency checks we can do to increase the confidence in our result and to better understand the nature of our evolution equations. We will pursue these cross-checks next in the following subsections, where we will justify the neighbor dipole amplitude following virtual correction in the evolution of Fig. 3 and successfully rederive the small-x polarized DGLAP anomalous dimension $\Delta P_{GG}(z \to 0)$ at NLO. Further comparison with the calculation by BER can be found in Appendix B.

D. Cross-check: Virtual diagrams and real-virtual cancellations

1. Evolution subsequent to a virtual correction

First we would like to cross-check and clarify the origin of the neighbor dipole amplitude Γ in the last term of the integrand in both Eqs. (16). These terms arise from the evolution subsequent to the virtual corrections in the last

[2]There is a caveat here: our result (21) for the intercept was calculated in the large-N_c pure-glue limit; the part of the calculation in [18] leading to the intercept $\alpha_h^{\text{BER}} = 3.66\sqrt{\frac{\alpha_s N_c}{2\pi}}$ was for the pure glue case, but was not in the large-N_c limit. Therefore one could attribute the difference between the two numbers to the difference between the large-N_c limit (us) and $N_c = 3$ (BER). To explore this possibility we have reproduced BER's solution for pure glue obtaining

$$\alpha_h^{\text{BER}} = \sqrt{\frac{17 + \sqrt{97}}{2}} \sqrt{\frac{\alpha_s N_c}{2\pi}} \approx 3.66 \sqrt{\frac{\alpha_s N_c}{2\pi}}. \tag{23}$$

Hence 3.66 is a pure number and this result holds for any N_c in the BER framework. Therefore, disagreement between the BER intercept and ours in Eq. (21) is not due to the large-N_c limit employed in our case.

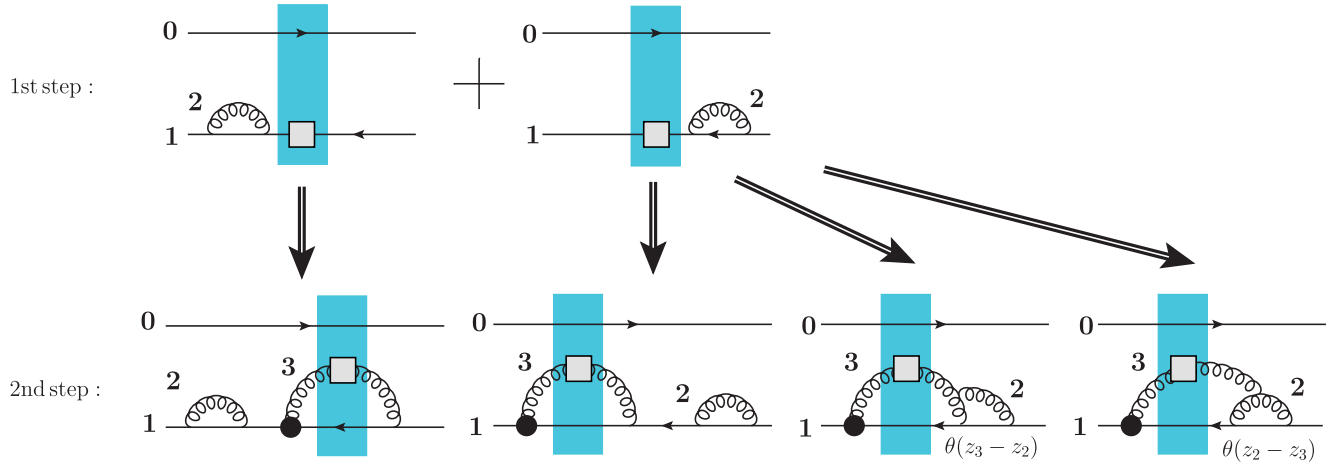

FIG. 4. Two steps of helicity evolution. In the first step, we consider BFKL-like virtual corrections (last 2 diagrams in Fig. 3). In the second step, we consider one particular type of correction, the emission of a soft polarized gluon (first diagram in Fig. 3), connected in all possible ways. The last two diagrams differ only in the time-ordering of the vertices.

two diagrams of the bottom line in Fig. 3. The real correction (leftmost diagram in the bottom line of Fig. 3) imposes a lifetime ordering constraint (19) on further DLA evolution of the dipole 21, while naively it seems that the virtual corrections (two rightmost diagrams in the bottom line of Fig. 3) impose no such constraint. As we shall see, the virtual diagrams actually *do* impose the same lifetime ordering condition in order for the subsequent evolution to remain DLA: to see this we need to perform a calculation.

Consider one particular step of subsequent DLA evolution following the virtual corrections, as shown in Fig. 4: the emission of a soft polarized gluon. One may have a ladder-type correction, as shown in the first two diagrams of the second line of Fig. 4. Or one may have a non-ladder-type correction with the polarized gluon attaching to the virtual gluon, as shown in the last two diagrams. Let us choose $z_2 \gg z_3$ for specificity (one step of evolution) and compute these diagrams explicitly in LFPT to see exactly what the DLA regime of the second evolution step is. We will work in the large-N_c limit, which is the context in which our evolution equations (16) and (20) are derived.

The polarized dipole amplitude $\mathcal{A}_{10}$ generated by the three diagrams shown in Fig. 5 is given by

$$\begin{aligned}\mathcal{A}_{10} = \int \frac{dq^+}{4\pi q^+} d^2x_3 \sum_{\text{colors}} \sum_{\lambda\sigma'} \langle U_{\underline{3}}(\lambda) V_{\underline{1}}^\dagger(\sigma')\rangle \left(\frac{q^+}{p^+}\right) \\ \times \left[\mathcal{V} \times \tilde{\psi}^{\text{pol}}_{\text{LO}}\left(\underline{x}_{31}, \frac{q^+}{p^+}\right) \times \left(-\tilde{\psi}^{\text{unp}}_{LO}\left(\underline{x}_{31}, \frac{q^+}{p^+}\right)\right)^* \right. \\ + \tilde{\psi}^{\text{pol}}_{LO}\left(\underline{x}_{31}, \frac{q^+}{p^+}\right) \times \left(-\tilde{\psi}^{\text{unp}}_{LO}\left(\underline{x}_{31}, \frac{q^+}{p^+}\right)\right)^* \mathcal{V}^* \\ \left. + \tilde{\psi}^{\text{pol}}_{LO}\left(\underline{x}_{31}, \frac{q^+}{p^+}\right) \times \left(-\tilde{\psi}^{\text{unp}}_{\text{NLO}}\left(\underline{x}_{31}, \frac{q^+}{p^+}\right)\right)^* \right],\end{aligned} \tag{24}$$

where $z_3 = \frac{q^+}{p^+}$ is the momentum fraction of the polarized gluon, and the notation is otherwise indicated in Fig. 5. The

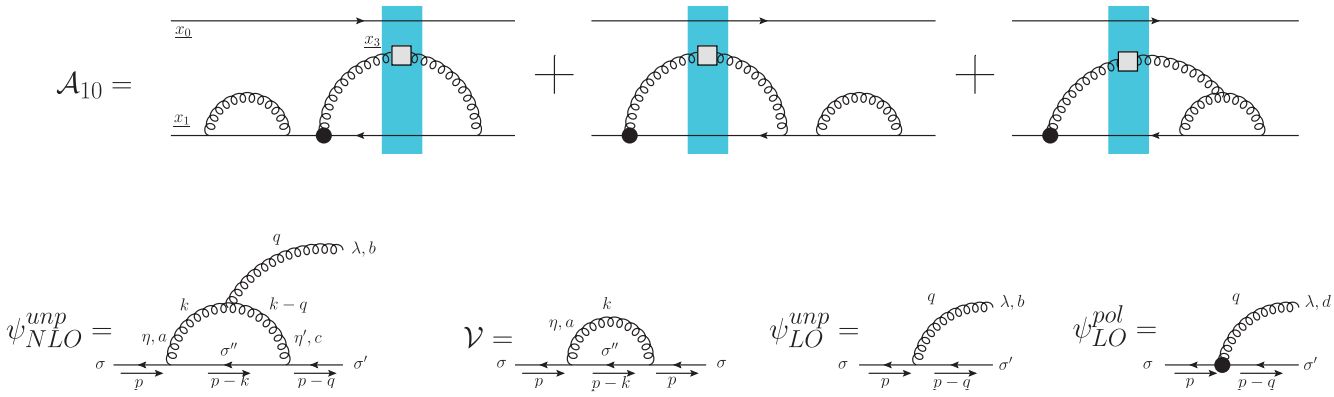

FIG. 5. Calculation of the light-front wave functions which go into the diagrams containing a virtual correction and a subsequent evolution step.

coordinate-space wave functions are related to the momentum-space wave functions by

$$\tilde{\psi}(\underline{x}_{31}, z_3) = \int \frac{d^2q}{(2\pi)^2} e^{i\underline{q}\cdot\underline{x}_{31}} \psi(\underline{q}, z_3), \tag{25}$$

which are calculated in the conventions of [17]. Here and below LO stands for leading order, NLO stands for next-to-leading order, etc. The virtual correction $\mathcal{V}$ is obtained by unitarity, requiring that the sum of $\mathcal{O}(\alpha_s)$ corrections to the (anti)quark wave function not modify the normalization,

$$\mathcal{V} = \mathcal{V}^* = -\frac{1}{2} \sum_{\text{colors}} \sum_{\sigma'' \eta} \int \frac{dz_2}{4\pi z_2} \frac{d^2k_2}{(2\pi)^2} |\psi^{\text{unp}}_{\text{LO}}(\underline{k}_2, z_2)|^2. \tag{26}$$

Using this to simplify (24), we obtain

$$\begin{aligned} \mathcal{A}_{10} = &- \int \frac{dz_3}{4\pi z_3} d^2x_3 \sum_{\text{colors}} \sum_{\lambda\sigma'} \lambda \tilde{\psi}^{\text{pol}}_{\text{LO}}(\underline{x}_{31}, z_3) \\ &\times \frac{1}{z_3 s} \langle\langle U^{\text{pol}}_{\underline{3}} V^\dagger_{\underline{1}} \rangle\rangle (z_3) \\ &\times [2\mathcal{V} \tilde{\psi}^{\text{unp}}_{\text{LO}}(\underline{x}_{31}, z_3) + \tilde{\psi}^{\text{unp}}_{\text{NLO}}(\underline{x}_{31}, z_3)]^*, \end{aligned} \tag{27}$$

and the real-virtual cancellations are contained within the sum in brackets.

The first term is straightforward to calculate using (26),

$$\begin{aligned} 2\mathcal{V} \tilde{\psi}^{\text{unp}}_{\text{LO}}(\underline{x}_{31}, z_3) = &\frac{ig^3 N_c}{(2\pi)^3} t^b \delta_{\sigma\sigma'} \frac{\underline{\epsilon}^*_\lambda \cdot \underline{x}_{32}}{x^2_{32}} \int_{z_3}^{z_1} \frac{dz_2}{z_2} \\ &\times \int_{1/z_2 s}^{x^2_{10} \frac{z_1}{z_2}} \frac{dx^2_{21}}{x^2_{21}}, \end{aligned} \tag{28}$$

where the DLA part comes from the regime $z_1 \gg z_2 \gg z_3$ and $x^2_{10} z_1 \gg x^2_{21} z_2$, with no apparent further constraint on x_{32}. Note that the sign of (28) is important, and one must correctly incorporate the sign for antiquark vertices [see, e.g., rule 3 following Eq. (3.28) of [50]]. We have also written the color factor $C_F \approx N_c/2$ in the large-N_c limit. Meanwhile, for the second term, we have in momentum space

$$\begin{aligned} \psi^{\text{unp}}_{\text{NLO}}(\underline{q}, z_3) = &-g^3 N_c t^b \frac{\underline{\epsilon}^*_\lambda \cdot \underline{q}}{q^2_T} \int_{z_3}^{z_1} \frac{dz_2}{(z_2)^2} \\ &\times \int \frac{d^2k}{(2\pi)^3} \frac{\underline{k} \cdot (\underline{k} - \underline{q})}{k^2_T} \left(\frac{q^2_T}{2z_3} + \frac{(k-q)^2_T}{2z_2} \right)^{-1} \end{aligned} \tag{29}$$

which is only DLA if $(k-q)^2_T \gg \frac{z_2}{z_3} q^2_T \gg q^2_T$. In coordinate space, this corresponds to $x^2_{21} \ll \frac{z_3}{z_2} x^2_{32} \ll x^2_{32} \approx x^2_{31}$, giving the DLA part as

$$\begin{aligned} \tilde{\psi}^{\text{unp}}_{\text{NLO}}(\underline{x}_{31}, z_3) = &-\frac{ig^3 N_c}{(2\pi)^3} t^b \frac{\underline{\epsilon}^*_\lambda \cdot \underline{x}_{31}}{x^2_{31}} \int_{z_3}^{z_1} \frac{dz_2}{z_2} \\ &\times \int_{1/z_2 s}^{x^2_{10} \frac{z_1}{z_2}} \frac{dx^2_{21}}{x^2_{21}} \theta(z_3 x^2_{31} - z_2 x^2_{21}). \end{aligned} \tag{30}$$

We see that in the regime $z_3 x^2_{31} \gg z_2 x^2_{21}$ (and for $z_2 \gg z_3$), all three diagrams of $\mathcal{A}_{10}$ are DLA and cancel so that $\mathcal{A}_{10} \approx 0$ with DLA accuracy. This means that the second step of evolution which produces the gluon $\underline{x}_3$ is actually *not* DLA in the whole phase space; the only DLA phase space which survives these cancellations is $z_3 x^2_{31} \ll z_2 x^2_{21}$ (again, for $z_2 \gg z_3$). Therefore, when we write the BFKL-type virtual corrections as in the first line of Fig. 4 (or in the right two diagrams of the second line of Fig. 3), we see that the subsequent DLA evolution of the dipole 10 implicitly has the condition $z_3 x^2_{31} \ll z_2 x^2_{21}$ imposed on it, so that the dipole amplitude is not $G_{10}(z_2)$, but rather the *neighbor dipole amplitude* $\Gamma_{10,21}(z_2)$. This is the reason why the virtual corrections [last terms of (16a) and (16b)] enter with the neighbor dipole constraint on their evolution.

2. Virtual corrections and unitarity

For completeness, let us study the case of opposite ordering, $z_3 \gg z_2$. Consider the two steps of DLA evolution in the opposite order: first the emission of a soft polarized gluon 3, followed by a BFKL-type correction (gluon 2) in the 01/03 dipoles included in all possible ways. In this case there are many possible virtual corrections to consider (Fig. 6, diagrams *A*—*F*) and two real corrections (Fig. 7, diagrams *G*—*H*). For ease of comparison with Fig. 5, we keep the polarized soft gluon to be at position $\underline{x}_3$ with momentum q and the BFKL-like unpolarized gluon to be at position $\underline{x}_2$ with momentum k. This ordering of the two evolution steps then corresponds to $\frac{q^+}{k^+} = \frac{z_3}{z_2} \gg 1$.

There are two separate DLA regimes for the graphs in Figs. 6 and 7, which are easily understood in the language of LFPT. The light-front energy (minus momentum) $E_2(E_3)$ of gluon 2(3) is directly related to the lifetimes of the gluon fluctuation; in coordinate space, these energies are: $E_2 = \frac{1}{z_2 x^2_{21}}$ for diagrams *A*, *B*, *E*, *F*, and *H*; $E_2 = \frac{1}{z_2 x^2_{23}}$ for diagrams *C*, *C*′, *D*, *D*′, and *G*; and $E_3 = \frac{1}{z_3 x^2_{31}}$ for all diagrams. (For brevity, in light-front energies we dropped the overall factor of $1/p^+$ with p^+ the probe's momentum.) As a rule of thumb, the two steps of evolution shown here are DLA when there is a well-separated hierarchy of lifetimes, such that the light-front energy of each gluon 2 and 3 dominates exactly two of the intermediate states, $E_2 \gg E_3$ or $E_3 \gg E_2$. (The application of this rule gets more nuanced for diagrams with virtual corrections.)

For $E_2 \gg E_3$, all the diagrams in Figs. 6 and 7 can be DLA except for the real diagram *H*. We would like to

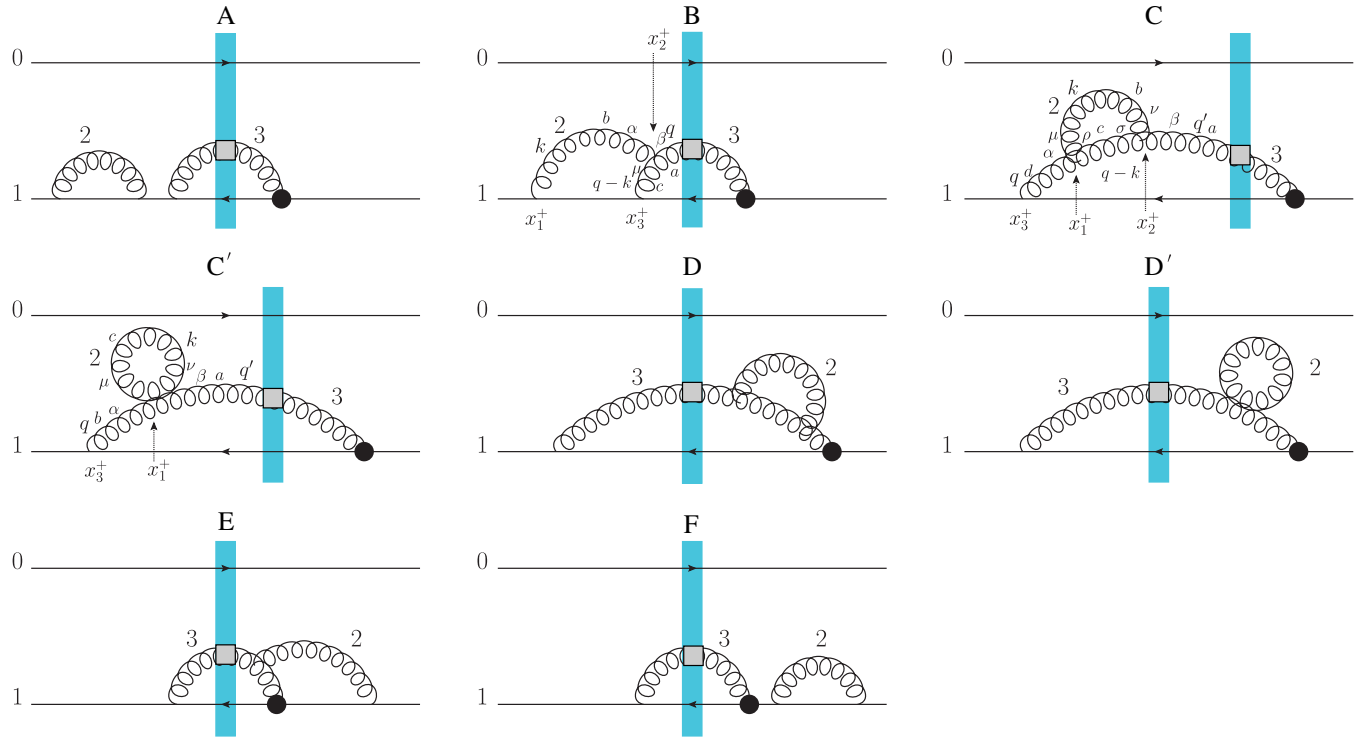

FIG. 6. DLA diagrams in which a BFKL-like virtual correction follows the real emission of a soft polarized gluon. We only consider diagrams which contribute to the further evolution of the (01) and (03) dipoles.

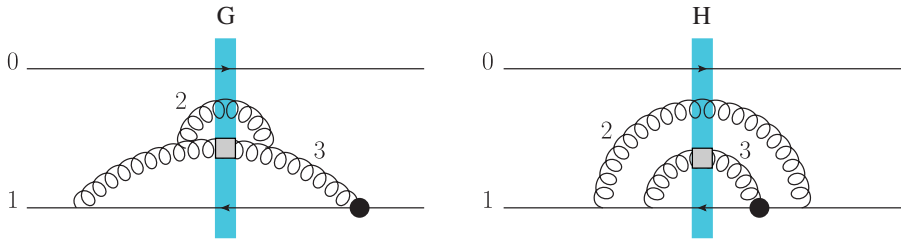

FIG. 7. DLA diagrams in which a BFKL-like real correction follows the real emission of a soft polarized gluon. We only consider diagrams which contribute to the further evolution of the (01) and (03) dipoles.

compute the sum of the virtual diagrams A—F in order to assess the cancellations which may occur between them. To do this, we will calculate the relevant parts of diagrams B, C, and C'; the analogous calculation of diagrams D, D' and E is almost equivalent, the small difference being due to the position of the polarized vertex to the right of the shock wave. It is convenient to do these calculations in Feynman perturbation theory, rather than in LFPT directly, treating the quark propagators as Wilson lines. To impose the corresponding time ordering, we need to Fourier transform each gluon propagator from k^- momentum space to x^+ coordinate space, and then integrate over all light cone "times" of the vertices x_i^+ with the ordering prescribed by the diagram.

We can apply this scheme to just the parts of diagrams B, C, C' which involve the radiation of gluons to the left of the shock wave; everything else is common to the three diagrams. Doing this, we obtain

$$B = \int_{-\infty}^{0} dx_1^+ \int_{x_1^+}^{0} dx_3^+ \int_{x_3^+}^{0} dx_2^+ e^{\epsilon(x_1^+ + x_2^+ + x_3^+)} \int_{-\infty}^{\infty} \frac{dk^-}{2\pi} \frac{dq^-}{2\pi} \frac{d(q-k)^-}{2\pi} \times e^{-ik^-(x_2^+ - x_1^+) - i(q-k)^-(x_2^+ - x_3^+) + iq^- x_2^+} \times \hat{B}, \tag{31a}$$

$$C=\int_{-\infty}^{0}dx_3^+\int_{x_3^+}^{0}dx_1^+\int_{x_1^+}^{0}dx_2^+\,e^{\epsilon(x_1^++x_2^++x_3^+)}\int_{-\infty}^{\infty}\frac{dk^-}{2\pi}\frac{dq^-}{2\pi}\frac{d(q-k)^-}{2\pi}\frac{dq'^-}{2\pi}\times e^{-ik^-(x_2^+-x_1^+)-i(q-k)^-(x_2^+-x_1^+)+iq'^-x_2^+-iq^-(x_1^+-x_3^+)}\times\hat{C}, \tag{31b}$$

$$C'=\int_{-\infty}^{0}dx_3^+\int_{x_3^+}^{0}dx_1^+\,e^{\epsilon(x_1^++x_3^+)}\int_{-\infty}^{\infty}\frac{dk^-}{2\pi}\frac{dq^-}{2\pi}\frac{dq'^-}{2\pi}\,e^{iq'^-x_1^+-iq^-(x_1^+-x_3^+)}\times\hat{C}'. \tag{31c}$$

In (31), we use the regulator $e^{\epsilon x^+}$ for positive infinitesimal ϵ to ensure convergence at $x^+\to-\infty$ (see e.g. [51]). The shock wave (interaction with the target) is taken to occur at $x^+=0^+$. The momentum-space expressions, calculated in Feynman perturbation theory, are

$$\hat{B}=(-ig)^2gf^{abc}t^bt^c\left(\frac{-i}{k^2+i\delta}\right)\left(\frac{-i}{(q-k)^2+i\delta}\right)\left(\frac{i\epsilon_\lambda^{*\beta}(q)}{q^2+i\delta}\right)\left[g^{-\alpha}-\frac{k^\alpha+g^{+\alpha}k^-}{k^+}\right]\left[g^{-\mu}-\frac{(q-k)^\mu+g^{+\mu}(q-k)^-}{q^+-k^+}\right]$$
$$\times[(2k-q)_\beta g_{\mu\alpha}-(q+k)_\mu g_{\alpha\beta}+(2q-k)_\alpha g_{\mu\beta}], \tag{32a}$$

$$\hat{C}=\frac{-ig^3}{2}f^{abc}f^{cbd}t^d\left(\frac{-i}{k^2+i\delta}\right)\left(\frac{-i}{q^2+i\delta}\right)\left(\frac{-i}{(q-k)^2+i\delta}\right)\left(\frac{i\epsilon_\lambda^{*\beta}(q')}{q'^2+i\delta}\right)$$
$$\times\left[g^{-\alpha}-\frac{q^\alpha+g^{+\alpha}q^-}{q^+}\right]\left[g^{\mu\nu}-\frac{k^\mu g^{+\nu}+k^\nu g^{+\mu}}{k^+}\right]\left[g^{\rho\sigma}-\frac{(q-k)^\rho g^{+\sigma}+(q-k)^\sigma g^{+\rho}}{q^+-k^+}\right]$$
$$\times[(2k-q)_\alpha g_{\mu\rho}-(q+k)_\rho g_{\mu\alpha}+(2q-k)_\mu g_{\alpha\rho}][(2k-q)_\beta g_{\sigma\nu}-(q'+k)_\sigma g_{\nu\beta}+(q+q'-k)_\nu g_{\sigma\beta}], \tag{32b}$$

$$\hat{C}'=(-g^3)\frac{N_c}{2}t^a\left(\frac{-i}{q^2+i\delta}\right)\left(\frac{-i}{k^2+i\delta}\right)\left(\frac{i\epsilon_\lambda^{*\beta}(q')}{q'^2+i\delta}\right)\left[g^{-\alpha}-\frac{q^\alpha+g^{+\alpha}q^-}{q^+}\right]\left[g^{\mu\nu}-\frac{g^{+\nu}k^\mu+g^{+\mu}k^\nu}{k^+}\right]$$
$$\times[2g_{\mu\nu}g_{\alpha\beta}-g_{\mu\beta}g_{\nu\alpha}-g_{\mu\alpha}g_{\nu\beta}]. \tag{32c}$$

In (32), we use $i\delta$ for the regulator of the Feynman propagator, and we have split (the numerator of) the propagator of gluon 3 through the shock wave into a polarization sum, keeping only the gluon polarization ϵ_λ^*. Note that diagrams C and C' come with an explicit minus sign due to the antiquark/gluon vertex [see (28) and the discussion thereafter] and that only half of their color factor "belongs" to the evolution of dipole 03 under consideration, the other half being the evolution in the dipole 31 which we do not consider here.

Keeping only the leading-energy, DLA part of the expressions, we obtain[3]

$$B=g^3\frac{N_c}{2}t^a\frac{1}{2k^+q^+k_\perp^2q_\perp^2}[\underline{\epsilon}_\lambda^*\cdot(-4\underline{q}+2\underline{k})], \tag{33a}$$

$$C=g^3\frac{N_c}{2}t^a\frac{1}{2k^+q^+k_\perp^2q_\perp^2}[\underline{\epsilon}_\lambda^*\cdot(4\underline{q}-2\underline{k})], \tag{33b}$$

$$C'=0. \tag{33c}$$

[3]Indeed diagram C' contains a UV divergence, which has to be canceled by a counterterm. This contribution is not DLA and is not shown in Eqs. (33).

Thus we see that, with DLA accuracy, $B+C+C'=0$. By an analogous calculation, one also finds that $D+D'+E=0$. The result is that, for $E_2\gg E_3$, only the virtual diagrams A, F from Fig. 6 and the real diagram G from Fig. 7 contribute to the DLA evolution of dipole 01 followed by the LLA-type evolution of dipole 03. Note that the latter LLA-type step comes with the $E_2\gg E_3$ condition, normally not associated with the LLA evolution.

On the other hand, in the $E_3\gg E_2$ regime, only the virtual diagrams A, F from Fig. 6 and the real diagram H from Fig. 7 are DLA. In this kinematic regime, we have $x_{21}^2\gg\frac{z_3}{z_2}x_{31}^2\gg x_{31}^2$ so that the dipole 31 is very small: gluon 3 is very close to the parent antiquark 1. Diagram H becomes indistinguishable from diagram G, since gluon 2 is essentially emitted from coordinate x_3 in both cases. Diagrams A, F and H then contribute to LLA-type evolution in the dipole $01\approx03$, now with the $E_3\gg E_2$ condition. Combining this with the contributions of diagrams A, F and G in the $E_2\gg E_3$ regime we obtain LLA evolution in the dipole 03 without any ordering of the light cone energies, as is normal for the LLA evolution. Such contribution is included in Eqs. (16).

The result of this analysis is that, in either DLA limit $E_2\gg E_3$ or $E_3\gg E_2$, one is left only with the virtual corrections A, F and the (equivalent) real correction G/H.

These BFKL-like real and virtual corrections are exactly the ones included in our evolution equation (15) and Fig. 3. And, moreover, in the absence of *any* interactions with the shock wave, $V, V^{\rm pol} = 1$, these real and virtual corrections cancel exactly [see (26)], as demanded by unitarity. Therefore we conclude that our treatment of BFKL-like virtual corrections exhausts the unitarity sum (with DLA accuracy), completing the cross-check of the way we have implemented these *unpolarized* radiative corrections to the polarized dipole amplitude.

E. Cross-check: DGLAP anomalous dimensions

Another important cross-check of our evolution equations is to verify that they reproduce the correct DGLAP anomalous dimensions at NLO accuracy. This is especially important in reconciling our disagreement with BER, since in Eq. (4.25) of their work [18], BER show that they reproduce the complete LO and NLO DGLAP polarized anomalous dimensions. (In addition, it was recently shown that the result of BER's formalism, expanded to higher orders in [52], correctly reproduces the NNLO polarized anomalous dimensions [53].) For BER, obtaining anomalous dimensions is a straightforward application of their infrared evolution equations which resum the mixed logarithms $\alpha_s^i (\ln \frac{1}{x})^{2i-j} (\ln \frac{Q^2}{\mu^2})^j$ for $0 \le j \le i$, such that their final answer contains all-order small-x anomalous dimensions for DGLAP evolution. One simply needs to expand this anomalous dimension to order α_s^2 to obtain the small-x contribution to the NLO anomalous dimension.

In our case, the correspondence is less clear, chiefly because, unlike BER, we do not have an exact analytic solution for our evolution equations and our evolution only resums powers of $\alpha_s \ln^2 \frac{1}{x}$. In addition, our equations do not close in general [see (15)], and, hence, cannot be used to easily extract the anomalous dimension of any of the involved operators. However, our large-N_c equations (in the flavor singlet case) close. Moreover, they can be written as a single closed equation for the expectation value of only one operator. Noting that the integrands are the same in (20), we formulate the evolution equations in terms of the linear combination

$$H(x_T^2, y_T^2, z) \equiv \Gamma(x_T^2, y_T^2, z) + 3G(y_T^2, z), \tag{34}$$

giving

$$\begin{aligned} H(x_{10}^2, x_{21}^2, z) &= G^{(0)}(x_{10}^2, z) + 3G^{(0)}(x_{21}^2, z) \\ &+ \frac{\alpha_s N_c}{2\pi} \int_{\frac{1}{x_{10}^2 s}}^{z} \frac{dz'}{z'} \int_{\frac{1}{z's}}^{\min\left[x_{10}^2, x_{21}^2 \frac{z}{z'}\right]} \frac{dx_{32}^2}{x_{32}^2} H(x_{10}^2, x_{32}^2, z') \\ &+ 3\frac{\alpha_s N_c}{2\pi} \int_{\frac{1}{x_{21}^2 s}}^{z} \frac{dz'}{z'} \int_{\frac{1}{z's}}^{x_{21}^2} \frac{dx_{32}^2}{x_{32}^2} H(x_{21}^2, x_{32}^2, z'). \end{aligned} \tag{35}$$

The resulting Eq. (35) contains only gluon bremsstrahlung, so we only have access to the glue-glue sector of the splitting kernel in the large-N_c approximation. (Our flavor-singlet helicity evolution equations also close in the large-N_c & N_f limit [29]; however, the resulting closed equations depend on the expectation values of several operators. We leave it for the future work to elucidate the possibility of extracting small-x polarized NLO DGLAP anomalous dimensions in the quark-quark, quark-gluon and gluon-quark sectors from those equations.)

DGLAP evolution expresses a PDF $f_i(x, Q^2)$ at one (UV) scale Q^2 and momentum fraction x in terms of a convolution of PDF's at lower (IR) scales $\mu^2 < k_T^2 < Q^2$ and higher momentum fractions $x' \ge x$,

$$\begin{aligned} f_i(x, Q^2) &= f_i(x, \mu^2) \\ &+ \int_x^1 \frac{dx'}{x'} \int_{\mu^2}^{Q^2} \frac{dk_T^2}{k_T^2} P_{i/j}\left(\frac{x}{x'}\right) f_j(x', k_T^2). \end{aligned} \tag{36}$$

The splitting functions are expanded in a perturbation series in α_s,

$$P_{i/j}(z) = P_{i/j}^{\rm LO}(z) + P_{i/j}^{\rm NLO}(z) + \cdots, \tag{37}$$

where the LO term is $\mathcal{O}(\alpha_s)$, the NLO term is $\mathcal{O}(\alpha_s^2)$, etc.

Our integral evolution equations, however, express the evolution "in the opposite direction" to standard DGLAP evolution. They express a polarized dipole distribution at one (IR) scale μ^2 and momentum fraction x in terms of a convolution of dipole distributions at *higher (UV)* scales $\mu^2 < \frac{1}{x_{21}^2} < Q^2$ and *lower* momentum fractions $x' \le x$. For example,

$$\begin{aligned} G\left(\frac{1}{\mu^2}, x\right) &= G^{(0)}\left(\frac{1}{\mu^2}, x\right) + \frac{\alpha_s N_c}{2\pi} \int_{\frac{\mu^2}{s}}^{x} \frac{dx'}{x'} \int_{\left(\frac{x}{x'}\right)\frac{1}{Q^2}}^{\frac{1}{\mu^2}} \frac{dx_{21}^2}{x_{21}^2} \\ &\times \left[\Gamma\left(\frac{1}{\mu^2}, x_{21}^2, x'\right) + 3G(x_{21}^2, x')\right], \end{aligned} \tag{38}$$

where we take $x = \frac{Q^2}{s}$ as in deep inelastic scattering at small x.

Clearly it would be difficult to recast our evolution equations into a form which can be easily compared to DGLAP. However, the *kernels* or *splitting functions* of the two equations should be comparable with one another, since they are built at the fundamental level from the same ingredients: the light-front splitting wave functions of quarks and gluons. Our strategy, then, will be to iterate our Eq. (35) to the desired order, since it is a closed equation for a single function H, translate the result into DGLAP kinematics, and then extract the splitting function from it.

Our DLA evolution equations generate two logarithms of energy after each step of evolution is completely integrated; when these double logarithms of energy are

translated from helicity evolution in Regge kinematics to DGLAP evolution in Bjorken kinematics, some of them will correspond to $\alpha_s \ln\frac{Q^2}{\mu^2}\ln\frac{1}{x}$ and others will correspond to $\alpha_s \ln^2\frac{1}{x}$. The former category of terms is leading-logarithmic in Q^2 and thus contributes to the LO DGLAP anomalous dimension. The latter category of terms is subleading in Q^2 and thus suppressed in the DGLAP hierarchy $\ln\frac{Q^2}{\mu^2} \gg \ln\frac{1}{x}$. The NLO anomalous dimension, therefore, comes from terms of order $\alpha_s^2 \ln\frac{Q^2}{\mu^2}\ln^3\frac{1}{x}$ and requires two iterations of our evolution equation to compute. Terms which contain no logarithms of Q^2, that is $(\alpha_s \ln^2\frac{1}{x})^n$, contribute to our evolution equation but not DGLAP evolution. Note that one logarithm of $\frac{1}{x}$ and one logarithm of Q^2 are contained in the explicit integral in (36), so that the NLO terms of interest in the splitting function P are of order $\alpha_s^2 \ln^2\frac{1}{x}$.

There is one further complication which is specific to our evolution equations: due to the "neighbor dipole" functions, the amplitude H which evolves in (35) depends on two scales (x_{01}^2 and x_{21}^2) rather than one like the PDF's and the DGLAP kernel. The reason behind this is that the neighbor dipole "remembers" one of the previous evolution steps. This makes it impossible to identify two steps of our evolution simply with two gluon emissions: the neighbor dipole takes into account at least one previous gluon emission. The problem here is in separating the NLO contribution coming from the two-gluon emission generated by two steps of helicity evolution (the result we want) from the admixture of the NLO contribution coming from the earlier gluon emission.

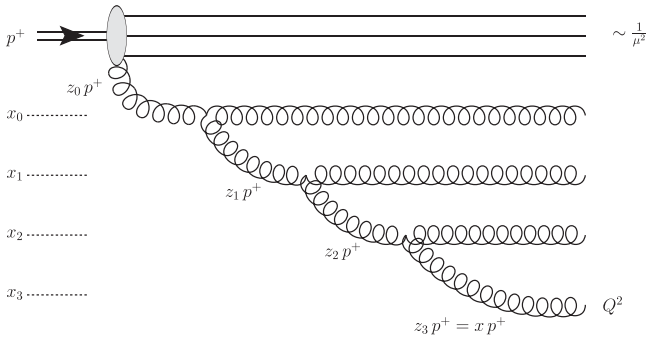

FIG. 8. Three gluon emissions, representing one step of the LO DGLAP-type evolution, followed by two steps of our DLA evolution, as suggested in Eq. (43).

The neighbor dipole is not directly observable; it only influences the evolution of the observable quantity $G(\frac{1}{\mu^2}, z_0)$. We could eliminate the above mentioned ambiguity by directly performing the first step of evolution in which the neighbor dipoles are generated,

$$G\left(\frac{1}{\mu^2}, z_0\right) = \frac{\alpha_s N_c}{2\pi}\int_{\frac{\mu^2}{s}}^{z_0}\frac{dz_1}{z_1}\int_{\frac{1}{z_1 s}}^{\frac{1}{\mu^2}}\frac{dx_{01}^2}{x_{01}^2} H\left(\frac{1}{\mu^2}, x_{01}^2, z_1\right), \tag{39}$$

where we have neglected the initial conditions, since they do not generate double logarithms. Then, performing two steps of H evolution by iterating (35), with all of the resulting emissions shown in Fig. 8, we obtain

$$\begin{aligned} G\left(\frac{1}{\mu^2}, z_0\right) = {} & \left(\frac{\alpha_s N_c}{2\pi}\right)^3 \int_{\frac{\mu^2}{s}}^{z_0}\frac{dz_1}{z_1}\int_{\frac{\mu^2}{s}}^{z_1}\frac{dz_2}{z_2}\int_{\frac{\mu^2}{s}}^{z_2}\frac{dz_3}{z_3}\int_{\frac{1}{z_1 s}}^{\frac{1}{\mu^2}}\frac{dx_{01}^2}{x_{01}^2} \\ & \times\left\{\int_{\frac{1}{z_2 s}}^{\min\left[\frac{1}{\mu^2}, \frac{x_{01}^2 z_1}{z_2}\right]}\frac{dx_{21}^2}{x_{21}^2}\left[\int_{\frac{1}{z_3 s}}^{\min\left[\frac{1}{\mu^2}, \frac{x_{21}^2 z_2}{z_3}\right]}\frac{dx_{32}^2}{x_{32}^2} H\left(\frac{1}{\mu^2}, x_{32}^2, z_3\right) + 3\theta\left(x_{21}^2 - \frac{1}{z_3 s}\right)\int_{\frac{1}{z_3 s}}^{x_{21}^2}\frac{dx_{32}^2}{x_{32}^2} H(x_{21}^2, x_{32}^2, z_3)\right]\right. \\ & \left. + 3\theta\left(x_{01}^2 - \frac{1}{z_2 s}\right)\int_{\frac{1}{z_2 s}}^{x_{01}^2}\frac{dx_{21}^2}{x_{21}^2}\left[\int_{\frac{1}{z_3 s}}^{\min\left[x_{01}^2, \frac{x_{21}^2 z_2}{z_3}\right]}\frac{dx_{32}^2}{x_{32}^2} H(x_{01}^2, x_{32}^2, z_3) + 3\theta\left(x_{21}^2 - \frac{1}{z_3 s}\right)\int_{\frac{1}{z_3 s}}^{x_{21}^2}\frac{dx_{32}^2}{x_{32}^2} H(x_{21}^2, x_{32}^2, z_3)\right]\right\}. \end{aligned} \tag{40}$$

Since we are interested only in two steps of DLA H evolution, we can replace $H \to 1$ to neglect further evolution in Eq. (40) and recast it into the form

$$G\left(\frac{1}{\mu^2}, z_0\right) = \int_{\frac{\mu^2}{s}}^{z_0}\frac{dz_3}{z_3}\mathcal{K}_{[\mathrm{DLA}^3]}\left(\frac{z_3}{z_0}, \frac{z_3 s}{\mu^2}\right). \tag{41}$$

We see that our evolution equation, like DGLAP evolution, can be expressed in the form of a convolution over a splitting kernel $\mathcal{K}(\frac{z_3}{z_0}, \frac{s}{\mu^2})$. Although our equations themselves are not comparable to DGLAP, this splitting kernel is. To make the comparison more explicit, we can analyze the kernel for fixed $z_3 = x = \frac{Q^2}{s}$, as appropriate for deep inelastic scattering at small x. We then have

$$\mathcal{K}_{[\mathrm{DLA}^3]}\left(\frac{x}{z_0},\frac{Q^2}{\mu^2}\right)=\left(\frac{\alpha_s N_c}{2\pi}\right)^3\int_x^{z_0}\frac{dz_1}{z_1}\int_x^{z_1}\frac{dz_2}{z_2}\int_{\frac{x}{z_1Q^2}}^{\frac{1}{\mu^2}}\frac{dx_{01}^2}{x_{01}^2}$$
$$\times\left\{\int_{\frac{x}{z_2Q^2}}^{\min\left[\frac{1}{\mu^2},\frac{x_{01}^2z_1}{z_2}\right]}\frac{dx_{21}^2}{x_{21}^2}\left[\int_{\frac{1}{Q^2}}^{\min\left[\frac{1}{\mu^2},\frac{x_{21}^2z_2}{x}\right]}\frac{dx_{32}^2}{x_{32}^2}+3\theta\left(x_{21}^2-\frac{1}{Q^2}\right)\int_{\frac{1}{Q^2}}^{x_{21}^2}\frac{dx_{32}^2}{x_{32}^2}\right]\right.$$
$$\left.+3\theta\left(x_{01}^2-\frac{x}{z_2Q^2}\right)\int_{\frac{x}{z_2Q^2}}^{x_{01}^2}\frac{dx_{21}^2}{x_{21}^2}\left[\int_{\frac{1}{Q^2}}^{\min\left[x_{01}^2,\frac{x_{21}^2z_2}{x}\right]}\frac{dx_{32}^2}{x_{32}^2}+3\theta\left(x_{21}^2-\frac{1}{Q^2}\right)\int_{\frac{1}{Q^2}}^{x_{21}^2}\frac{dx_{32}^2}{x_{32}^2}\right]\right\}. \quad (42)$$

There are, unfortunately, a couple of problems with directly extracting the NLO anomalous dimensions from this kernel. Foremost, the first step (39) is not a "diagonal" evolution like DGLAP: it connects two different functions G and H. Moreover, as we have suggested by labeling the kernel DLA^3, the integrals in this first step could potentially generate contributions to the NLO anomalous dimension, which would contaminate the "true" NLO kernel generated during the two steps of DLA evolution of H. We can resolve this problem by restricting this first step of evolution to the LO DGLAP phase space; that is, we can impose the strict transverse ordering $\frac{1}{Q^2}<x_{01}^2<\frac{1}{\mu^2}$ in Eq. (39). Thus, we can compute the modified kernel $\mathcal{K}_{[\mathrm{LO}\times\mathrm{DLA}^2]}$ for *three* steps of evolution,

$$G\overset{\mathrm{LO}}{\Rightarrow}H\overset{\mathrm{DLA}}{\Rightarrow}H\overset{\mathrm{DLA}}{\Rightarrow}H. \quad (43)$$

This eliminates the scale ambiguity coming from the neighbor dipoles, and it guarantees that the NLO anomalous dimension we compute arises purely from the "diagonal" evolution of H and can be connected to the NLO DGLAP anomalous dimension. The three steps of evolution (43) are illustrated diagrammatically in Fig. 8.

For completeness, we rewrite the modified kernel explicitly,

$$\mathcal{K}_{[\mathrm{LO}\times\mathrm{DLA}^2]}\left(\frac{x}{z_0},\frac{Q^2}{\mu^2}\right)=\left(\frac{\alpha_s N_c}{2\pi}\right)^3\int_x^{z_0}\frac{dz_1}{z_1}\int_x^{z_1}\frac{dz_2}{z_2}\int_{\frac{1}{Q^2}}^{\frac{1}{\mu^2}}\frac{dx_{01}^2}{x_{01}^2}$$
$$\times\left\{\int_{\frac{x}{z_2Q^2}}^{\min\left[\frac{1}{\mu^2},\frac{x_{01}^2z_1}{z_2}\right]}\frac{dx_{21}^2}{x_{21}^2}\left[\int_{\frac{1}{Q^2}}^{\min\left[\frac{1}{\mu^2},\frac{x_{21}^2z_2}{x}\right]}\frac{dx_{32}^2}{x_{32}^2}+3\theta\left(x_{21}^2-\frac{1}{Q^2}\right)\int_{\frac{1}{Q^2}}^{x_{21}^2}\frac{dx_{32}^2}{x_{32}^2}\right]\right.$$
$$\left.+3\int_{\frac{x}{z_2Q^2}}^{x_{01}^2}\frac{dx_{21}^2}{x_{21}^2}\left[\int_{\frac{1}{Q^2}}^{\min\left[x_{01}^2,\frac{x_{21}^2z_2}{x}\right]}\frac{dx_{32}^2}{x_{32}^2}+3\theta\left(x_{21}^2-\frac{1}{Q^2}\right)\int_{\frac{1}{Q^2}}^{x_{21}^2}\frac{dx_{32}^2}{x_{32}^2}\right]\right\}, \quad (44)$$

and we carry out the integrations employing DGLAP kinematics $\ln\frac{Q^2}{\mu^2}\gg\ln\frac{1}{x}$ to neglect the theta-function terms like $\theta(\frac{\mu^2}{Q^2}-\frac{x}{z_1})$, $\theta(\frac{\mu^2}{Q^2}-\frac{z_2}{z_1})$, etc. Such terms do not contribute to DGLAP evolution. After z-integrations they give terms proportional $\theta(\frac{\mu^2}{Q^2}-x)$ which may be identified as a higher-twist effect (see Sec. IV below for a further discussion of these terms). We arrive at

$$\mathcal{K}_{[\mathrm{LO}\times\mathrm{DLA}^2]}\left(\frac{x}{z_0},\frac{Q^2}{\mu^2}\right)=\left(\frac{\alpha_s N_c}{2\pi}\right)^3\left[\frac{4}{3}\ln^3\frac{Q^2}{\mu^2}\ln^2\frac{z_0}{x}+\frac{2}{3}\ln^2\frac{Q^2}{\mu^2}\ln^3\frac{z_0}{x}+\cdots\right], \quad (45)$$

where the ellipsis denote the terms with one or no logarithms of Q^2, which are not important for DGLAP evolution at the order of interest.

To claim that our kernel (45) is comparable with the DGLAP kernel, we need to explicitly make the connection with the LO and NLO DGLAP splitting functions. Only the diagonal evolution $H\overset{\mathrm{DLA}}{\Rightarrow}H\overset{\mathrm{DLA}}{\Rightarrow}H$ is compatible with DGLAP, containing both LO^2 and NLO contributions depending on the logarithms. That is, we claim that our kernel is related to DGLAP by

$$\mathcal{K}_{[\mathrm{LO}\times\mathrm{DLA}^2]}\left(\frac{x}{z_0},\frac{Q^2}{\mu^2}\right)=\frac{\alpha_s N_c}{2\pi}\int_x^{z_0}\frac{dz_1}{z_1}\int_{\frac{1}{Q^2}}^{\frac{1}{\mu^2}}\frac{dx_{01}^2}{x_{01}^2}\left[\mathcal{K}^{\mathrm{DGLAP}}_{[\mathrm{LO}^2]}\left(\frac{x}{z_1},x_{01}^2Q^2\right)+\mathcal{K}^{\mathrm{DGLAP}}_{[\mathrm{NLO}]}\left(\frac{x}{z_1},x_{01}^2Q^2\right)+\cdots\right]$$
$$=\frac{\alpha_s N_c}{2\pi}\int_x^{z_0}\frac{dz_1}{z_1}\int_{\frac{1}{Q^2}}^{\frac{1}{\mu^2}}\frac{dx_{01}^2}{x_{01}^2}\left[\int_x^{z_1}\frac{dz_2}{z_2}\int_{\frac{1}{Q^2}}^{x_{01}^2}\frac{dx_{32}^2}{x_{32}^2}\Delta P^{\mathrm{LO}}_{S,GG}\left(\frac{x}{z_2}\ll 1\right)\int_{x_{32}^2}^{x_{01}^2}\frac{dx_{21}^2}{x_{21}^2}\Delta P^{\mathrm{LO}}_{S,GG}\left(\frac{z_2}{z_1}\ll 1\right)\right.$$
$$\left.+\int_{\frac{1}{Q^2}}^{x_{01}^2}\frac{dx_{31}^2}{x_{31}^2}\Delta P^{\mathrm{NLO}}_{S,GG}\left(\frac{x}{z_1}\ll 1\right)\right] \tag{46}$$

where $\Delta P^{\mathrm{LO}}_{S,GG}$ and $\Delta P^{\mathrm{NLO}}_{S,GG}$ are the LO and NLO polarized glue/glue splitting functions, respectively.

To check this assertion, we can directly compute the LO^2 part of the splitting kernel, remembering that the LO glue-glue splitting function for polarized DGLAP evolution is $\Delta P^{\mathrm{LO}}_{S,GG}(z\to 0)=4N_c(\alpha_s/2\pi)$ [28] [which can also be derived from our Eq. (35)]. We obtain

$$\frac{\alpha_s N_c}{2\pi}\int_x^{z_0}\frac{dz_1}{z_1}\int_{\frac{1}{Q^2}}^{\frac{1}{\mu^2}}\frac{dx_{01}^2}{x_{01}^2}\mathcal{K}^{\mathrm{DGLAP}}_{[\mathrm{LO}^2]}\left(\frac{x}{z_1},x_{01}^2Q^2\right)$$
$$=\left(\frac{\alpha_s N_c}{2\pi}\right)^3\left[\frac{4}{3}\ln^3\frac{Q^2}{\mu^2}\ln^2\frac{z_0}{x}\right]. \tag{47}$$

We see that, indeed, this reproduces the $\mathcal{O}(\ln^3 Q^2)$ term of (45). This is an important cross-check of our calculation. Subtracting off this LO^3 piece,

$$\mathcal{K}_{[\mathrm{LO}\times\mathrm{DLA}^2-\mathrm{LO}^3]}\left(\frac{x}{z_0},\frac{Q^2}{\mu^2}\right)$$
$$\equiv\mathcal{K}_{[\mathrm{LO}\times\mathrm{DLA}^2]}\left(\frac{x}{z_0},\frac{Q^2}{\mu^2}\right)$$
$$-\frac{\alpha_s N_c}{2\pi}\int_x^{z_0}\frac{dz_1}{z_1}\int_{\frac{1}{Q^2}}^{\frac{1}{\mu^2}}\frac{dx_{01}^2}{x_{01}^2}\mathcal{K}^{\mathrm{DGLAP}}_{[\mathrm{LO}^2]}\left(\frac{x}{z_1},x_{01}^2Q^2\right)$$
$$=\frac{\alpha_s N_c}{2\pi}\int_x^{z_0}\frac{dz_1}{z_1}\int_{\frac{1}{Q^2}}^{\frac{1}{\mu^2}}\frac{dx_{01}^2}{x_{01}^2}\int_{\frac{1}{Q^2}}^{x_{01}^2}\frac{dx_{31}^2}{x_{31}^2}\Delta P^{\mathrm{NLO}}_{S,GG}\left(\frac{x}{z_1}\ll 1\right), \tag{48}$$

we can extract the NLO splitting function from (45) by differentiating,

$$\Delta P^{\mathrm{NLO}}_{S,GG}\left(\frac{x}{z_0}\ll 1\right)$$
$$=\frac{2\pi}{\alpha_s N_c}\frac{\partial}{\partial\ln\frac{z_0}{x}}\left(\frac{\partial}{\partial\ln\frac{Q^2}{\mu^2}}\right)^2\mathcal{K}_{[\mathrm{LO}\times\mathrm{DLA}^2-\mathrm{LO}^3]}\left(\frac{x}{z_0},\frac{Q^2}{\mu^2}\right). \tag{49}$$

Doing so, we obtain

$$\Delta P^{\mathrm{NLO}}_{S,GG}(z\to 0)|_{\text{pure glue}}=\left(\frac{\alpha_s}{2\pi}\right)^2 4N_c^2\ln^2 z \tag{50}$$

in complete agreement with the literature [32].

The corresponding anomalous dimension can be found using

$$\gamma(\omega)=\int_0^1 dz z^{\omega-1}\Delta P(z). \tag{51}$$

We obtain the pure-glue flavor-singlet anomalous dimension

$$\gamma^{\mathrm{NLO}}_{S,GG}(\omega)|_{\text{pure glue},\,\omega\to 0}=\left(\frac{\alpha_s}{2\pi}\right)^2\frac{8N_c^2}{\omega^3}, \tag{52}$$

also in agreement with [32].

We conclude that our helicity evolution generates the small-x flavor-singlet polarized DGLAP glue-glue splitting function and anomalous dimension, which are in complete agreement with the existing LO [28] and NLO calculations [32].

III. FLAVOR NONSINGLET HELICITY EVOLUTION

A. Flavor nonsinglet initial conditions

Let us now derive the evolution equations governing the small-x behavior of the flavor nonsinglet helicity distribution

$$\Delta q^{NS}(x,Q^2)\equiv\Delta q^f(x,Q^2)-\Delta\overline{q}^f(x,Q^2) \tag{53}$$

along with other flavor nonsinglet helicity observables. First of all, by analogy to the flavor singlet case, we need to define the observables. Again we consider the diagrams in Fig. 1. However, in the flavor nonsinglet case we need to *subtract* from them the same diagrams with the quark particle number flowing in the opposite direction in the quark loop. We obtain the following expressions for flavor nonsinglet helicity observables [cf. Eqs. (8)]:

$$g_1^{NS}(x,Q^2) = \frac{N_c}{2\pi^2\alpha_{\rm EM}}\int_{z_i}^1 \frac{dz}{z^2(1-z)} \times \int dx_{01}^2 \left[\frac{1}{2}\sum_{\lambda\sigma\sigma'}|\psi^T_{\lambda\sigma\sigma'}|^2_{(x_{01}^2,z)} + \sum_{\sigma\sigma'}|\psi^L_{\sigma\sigma'}|^2_{(x_{01}^2,z)}\right] \times G^{NS}(x_{01}^2,z), \tag{54a}$$

$$\Delta q^{NS}(x,Q^2) = \frac{N_c}{2\pi^3}\int_{z_i}^1 \frac{dz}{z}\int_{\frac{1}{zs}}^{\frac{1}{zQ^2}} \frac{dx_{01}^2}{x_{01}^2} G^{NS}(x_{01}^2,z), \tag{54b}$$

$$g_{1L}^{NS}(x,k_T^2) = \frac{8N_c}{(2\pi)^6}\int_{z_i}^1 \frac{dz}{z}\int d^2x_{01}d^2x_{0'1}e^{-i\underline{k}\cdot(\underline{x}_{01}-\underline{x}_{0'1})} \times \frac{\underline{x}_{01}\cdot\underline{x}_{0'1}}{x_{01}^2x_{0'1}^2} G^{NS}(x_{01}^2,z). \tag{54c}$$

Here we do not sum over flavors. Hence our expressions (54) should be understood as containing the contribution of one particular quark flavor. Since quark masses can be neglected in our DLA approximation, the small-x asymptotics of all helicity observables in (8) and (54) (flavor singlet and nonsinglet) is flavor-independent. Flavor dependence may reside in the initial conditions, but the asymptotic x dependence [the intercept α_h with $\Delta q \sim (\frac{1}{x})^{\alpha_h}$] should be independent of flavor.

Equations (54) contain the flavor nonsinglet polarized dipole amplitude defined by [cf. Eqs. (9)]

$$G_{10}^{NS}(z) \equiv \frac{1}{2N_c}\langle\!\langle \mathrm{tr}[V_{\underline{0}}V_{\underline{1}}^{\rm pol\dagger}] - \mathrm{tr}[V_{\underline{1}}^{\rm pol}V_{\underline{0}}^{\dagger}]\rangle\!\rangle(z) = G^{NS}(\underline{x}_1,\underline{x}_0,z) = G^{NS}(\underline{x}_{10},\underline{b},z), \tag{55a}$$

$$G^{NS}(x_{01}^2,z) \equiv \int d^2b\, G_{10}^{NS}(z). \tag{55b}$$

In Eqs. (54) we assume that the leading high-energy contribution to $G_{10}^{NS}(z)$ is real, such that $G_{10}^{NS}(z) = G_{10}^{NS*}(z)$.

To determine the initial conditions $G_{10}^{NS(0)}(z)$ for the flavor nonsinglet helicity evolution we use Eqs. (55a) and (11) to write

$$G_{10}^{NS}(z) = -\frac{zs}{2}\left(\frac{d\sigma}{d^2b}[q_{\underline{0}}^{unp},\Delta\overline{q}_{\underline{1}},zs] - \frac{d\sigma}{d^2b}[\overline{q}_{\underline{0}}^{unp},\Delta q_{\underline{1}},zs]\right). \tag{56}$$

Employing Eq. (56) we obtain for a single-quark target

$$G_{10}^{NS(0)} = \frac{\alpha_s^2(C_F)^2}{N_c}\frac{1}{x_1^2}, \tag{57a}$$

$$G^{NS(0)}(x_{10}^2,z) = \frac{\alpha_s^2(C_F)^2}{N_c}\pi\ln\frac{zs}{\Lambda^2}. \tag{57b}$$

In arriving at Eqs. (57) we had to subtract the contribution of the diagrams in the bottom row of Fig. 2 out of the contribution of the diagrams in the top row of the same figure. The last two diagrams in each row canceled, and the final answer in Eqs. (57) is given solely by the upper left graph in Fig. 2 with the t-channel quarks exchange. This makes clear physical sense: only quarks can transfer flavor information from the target to projectile. Therefore, quark exchange in the t-channel is necessary for the flavor nonsinglet observables.

Once again, the Born-level results (57) can be "dressed" by GM/MV multiple rescatterings

$$G_{10}^{NS(0)} = \frac{\alpha_s^2(C_F)^2}{N_c}\frac{1}{x_1^2}\exp\left[-\frac{1}{4}x_{10}^2Q_s^2(b)\ln\frac{1}{x_{01}\Lambda}\right]. \tag{58}$$

Either Eqs. (57) or (58) can be used as the initial conditions for flavor nonsinglet helicity evolution: if one wants to keep saturation effects in the initial conditions one should use (58), otherwise one should use (57).

B. Flavor nonsinglet helicity evolution at small x

To construct flavor nonsinglet helicity evolution equations, let us consider one step of small-x evolution. Looking at the diagrams in Fig. 3, we see immediately that the radiation of soft polarized gluons carries polarization information but not flavor and therefore does not contribute to the flavor nonsinglet distribution. Hence the first two diagrams on the right of the equation illustrated in Fig. 3 do not contribute.

Next we consider the unpolarized-gluon emission diagrams in the bottom row of Fig. 3. As we saw in deriving Eqs. (57), in the flavor nonsinglet case the unpolarized quark in the dipole amplitude does not interact in the initial conditions. Hence, if the shock wave in Fig. 3 represented the initial conditions only, the diagrams in the bottom row of that figure should cancel, as illustrated in Fig. 9. The

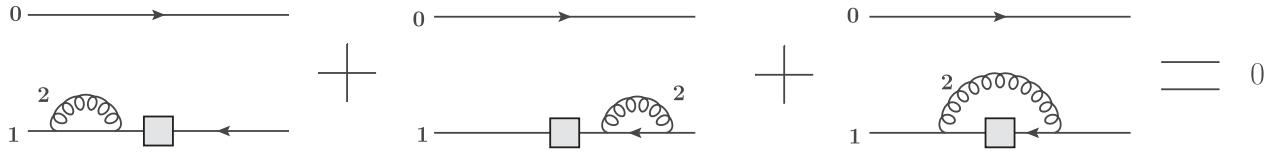

FIG. 9. Real-virtual cancellations of soft unpolarized gluon emissions in the flavor nonsinglet case (see [54]). In the strict DLA limit, only the polarized (anti)quark line interacts [as indicated by the absence of a shock-wave (blue rectangle)], and the sum of the real and virtual BFKL-like diagrams is zero.

same is true for the strict DLA evolution case: the cancellation of Fig. 9 is true at each step of the evolution, since it is true in the initial conditions.

If one wants to go beyond the strict DLA limit and use the saturation-enhanced initial conditions (58), then soft gluon in the rightmost diagram of Fig. 9 would interact with the target, and the cancellation would no longer be valid. However, since the dipole size x_{10} dependence in Eq. (58) is modified as compared to the Born-level Eqs. (57) (for the terms containing multiple rescatterings), the corresponding evolution is not going to be DLA and would be simply LLA BK/JIMWLK evolution in the dipole 01. In the large-N_c limit such LLA evolution in dipole 01 is included in the rightmost diagram in the top row of Fig. 3. One also has to include this LLA evolution into the initial conditions for the DLA evolution [25]. Let us stress one more time that such corrections are beyond the strict DLA limit.

We are left only with the rightmost diagram in the top row of Fig. 3 as contributing to the small-x evolution of the polarized dipole operator at small-x. Iteration of this diagram would give us a simple ladder with quarks in the t-channel and with gluon rungs (cf. [25]).

However, one should be careful here. We have never shown that the diagrams in Fig. 3 present all the possibilities for one step of the flavor nonsinglet helicity evolution. (Actually, diagrams in Fig. 3 illustrate the evolution in the flavor singlet case, as derived in [29].) In fact, for a step of the flavor nonsinglet evolution, the diagrams in Fig. 3 do not exhaust all the possibilities. Some of the flavor-singlet evolution diagrams not obtainable by evolution equations employing multiple applications of the diagrams in Fig. 3 (or, more precisely, in Figs. 11 and 12 of [29]) are shown in Fig. 10. These are nonladder diagrams which do not contribute to the flavor singlet case, and which are not included in Eq. (15). The diagrams in Fig. 10 are DLA and should appear after two steps of flavor nonsinglet helicity evolution.

It appears that in order to include the diagrams from Fig. 10 into the operatorial helicity evolution equations akin to (15) one may need to define a polarized "Wilson line" that starts as a gluon/quark on one side of the shock wave, and becomes a quark/gluon on the other side; examples of how such evolution could play out are shown in Fig. 10. These features will likely complicate the formalism; indeed, since such "identity-changing" Wilson lines occur in pairs, the evolution equations may be nonlinear. Luckily the diagrams in question are subleading in N_c and do not need to be considered in the large-N_c limit.

We proceed by imposing the large-N_c limit on the flavor nonsinglet helicity evolution. The resulting evolution equation receives contributions only from the quark ladder (third diagram on the right-hand side of Fig. 3); it is mathematically almost identical to the familiar Reggeon evolution equation known in the small-x literature [25]

$$G_{10}^{NS}(z) = G_{10}^{NS(0)}(z) + \frac{\alpha_s N_c}{4\pi} \int_{\frac{\Lambda^2}{s}}^{z} \frac{dz'}{z'} \int_{\frac{1}{z's}}^{x_{10}^2 \frac{z}{z'}} \frac{dx_{21}^2}{x_{21}^2} S_{10}(z') G_{21}^{NS}(z'). \quad (59)$$

This equation is illustrated diagrammatically in Fig. 11.

In Eq. (59) we again include the nonlinear LLA evolution effects by keeping $S_{10}(z')$, to be found from the BK/JIMWLK evolution, in the integrand. Note that the initial conditions can also include BK/JIMWLK-evolved S-matrix in place of the exponential in Eq. (58).

C. Solution of flavor nonsinglet helicity evolution equations at large N_c

In the strict DLA limit we put $S = 1$ everywhere, and Eq. (59) becomes

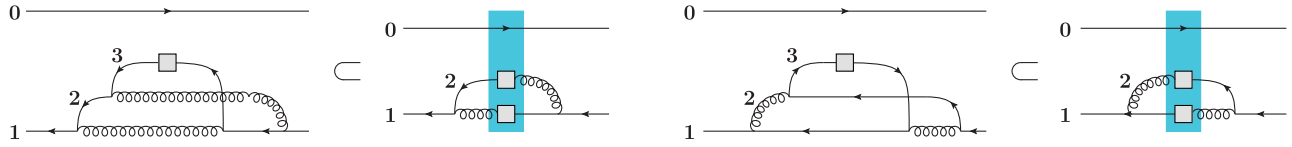

FIG. 10. Some of the nonladder diagrams contributing to the small-x flavor nonsinglet helicity evolution.

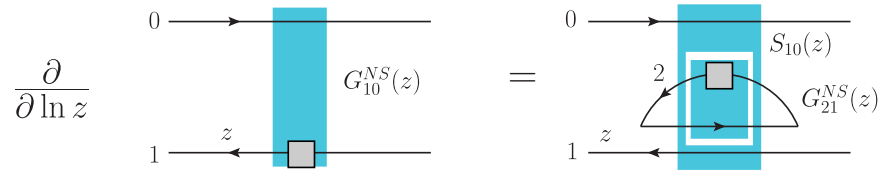

FIG. 11. Large-N_c evolution equation for the flavor nonsinglet polarized dipole amplitude. For simplicity, the initial conditions $G_{10}^{NS(0)}$ are not shown.

$$G_{10}^{NS}(z) = G_{10}^{NS(0)}(z) + \frac{\alpha_s N_c}{4\pi}\int_{\frac{\Lambda^2}{s}}^{z}\frac{dz'}{z'}\int_{\frac{1}{z's}}^{x_{10}^2\frac{z}{z'}}\frac{dx_{21}^2}{x_{21}^2}G_{21}^{NS}(z'). \quad (60)$$

Integrating over the impact parameters yields

$$G^{NS}(x_{10}^2, z) = G^{NS(0)}(x_{10}^2, z) + \frac{\alpha_s N_c}{4\pi}\int_{\Lambda^2/s}^{z}\frac{dz'}{z'}\int_{1/z's}^{x_{10}^2\frac{z}{z'}}\frac{dx_{21}^2}{x_{21}^2}G^{NS}(x_{21}^2, z'). \quad (61)$$

The Reggeon evolution equation (61) can be solved by the usual method of the Laplace-Mellin transform

$$G^{NS}(x_{10}^2, z) = \int\frac{d\omega}{2\pi i}e^{\omega\eta}\int\frac{d\lambda}{2\pi i}e^{\lambda s_{10}}G_{\omega\lambda}^{NS},$$
$$G_{\omega\lambda}^{NS} = \int_0^\infty d(\eta - s_{10})e^{-\lambda(\eta - s_{10})} \times \int_0^\infty d\eta e^{-\omega\eta}G^{NS}(x_{10}^2, z), \quad (62)$$

where the natural variables for the transform are

$$\eta \equiv \ln\frac{zs}{\Lambda^2} > 0 \qquad \eta' \equiv \ln\frac{z's}{\Lambda^2} > 0$$
$$s_{10} \equiv \ln\left(\frac{1}{x_{10}^2\Lambda^2}\right) < \eta \qquad s_{21} \equiv \ln\left(\frac{1}{x_{21}^2\Lambda^2}\right) < \eta'. \quad (63)$$

In terms of these variables, the flavor nonsinglet evolution equation is

$$G^{NS}(s_{10}, \eta) = G^{NS(0)}(s_{10}, \eta) + \frac{\alpha_s N_c}{4\pi}\int_0^\eta d\eta'\int_{s_{10}-\eta+\eta'}^{\eta'}ds_{21}G^{NS}(s_{21}, \eta'). \quad (64)$$

In Mellin space, the evolution equation is solved algebraically,

$$G_{\omega\lambda}^{NS} = \frac{1}{1 - (\frac{\alpha_s N_c}{4\pi})\frac{1}{\omega\lambda}}G_{\omega\lambda}^{NS(0)} = \frac{\alpha_s^2(C_F)^2\pi}{N_c\omega}\left(\frac{1}{\omega\lambda - \frac{\alpha_s N_c}{4\pi}}\right), \quad (65)$$

where the flavor nonsinglet initial condition comes from Eq. (57a). The large-(zs) asymptotics, evaluated in the saddle point approximation, are given by

$$G^{NS}(x_{10}^2, z) \propto (zs)^{\alpha_h^{NS}} \quad \text{with} \quad \alpha_h^{NS} = \sqrt{\frac{\alpha_s N_c}{\pi}}, \quad (66)$$

such that

$$g_1^{NS}(x, Q^2) \sim \Delta q^{NS}(x, Q^2) \sim g_{1L}^{NS}(x, k_T^2) \sim \left(\frac{1}{x}\right)^{\alpha_h^{NS}} \approx \left(\frac{1}{x}\right)^{\sqrt{\frac{\alpha_s N_c}{\pi}}}. \quad (67)$$

Note again that the intercept is flavor-independent at this leading order obtained by the DLA resummation.

This flavor nonsinglet intercept α_h^{NS}, calculated from solving our large-N_c nonsinglet helicity evolution equation (60), agrees exactly with the (large-N_c limit of the) result of BER's calculation [19] using the method of infrared evolution equations. Progress in incorporating nonlinear multiple scattering corrections to the Reggeon-like evolution equations like (59) has been made in the context of baryon number transport at small x [25].

IV. CONCLUSIONS

In this paper we have considered small-x asymptotics of the flavor singlet and nonsinglet helicity observables. We have defined the relations between the helicity TMD's, PDF's and g_1 structure functions to the polarized dipole operators in both flavor singlet and nonsinglet cases. The resulting difference in the polarized dipole operators can be seen in Eqs. (9a) and (55a). We have evaluated the polarized dipole amplitude in the MV model/GM approximation obtaining the initial conditions for the small-x evolution. We have then reconstructed evolution equations for the polarized dipole amplitude in the flavor singlet case originally derived in [29], filling in the important intermediate steps not presented in [29].

The solution of the large-N_c flavor singlet evolution equations, presented in [31], leads to the intercept in Eq. (21), which is about $2/3$ of the flavor singlet intercept obtained by BER in [18]. Our calculation satisfies all of the same cross-checks as BER (with the exception of the NNLO anomalous dimension for polarized DGLAP which we did not verify due to complexity of the calculation in our approach). Our effort to reproduce the calculation of BER working in Feynman gauge used in [18] is presented in Appendix B. At the moment it appears that BER might be missing parts of the DLA contributions of diagrams B, C, D, E and I from Fig. 12 in their calculation.

It is possible that, by omitting the DLA contributions discussed in our Appendix B, BER effectively restricted their analysis to the leading-twist evolution only [see Eq. (4.1) in [18]], or, at least discarded a subset of higher-twist terms. This assumption is consistent with the BER formalism generating correct anomalous dimensions for polarized DGLAP evolution, presently verified up to (and including) NNLO [53]. The disagreement between BER and our intercept may then be attributed to the fact that our evolution is all-twist, due to the terms like

$\theta(\frac{\mu^2}{Q^2} - x)$ which we include in our helicity evolution [see the discussion below Eq. (44) where such terms were mentioned, and neglected, but only in the DGLAP anomalous dimension calculation]. (The discontinuous nature of the theta-function terms is probably a property of DLA and is likely to be smoothed-out by higher-order corrections.) In the case of unpolarized BFKL evolution, which is all-twist, it is known that the exact all-twist intercept $\alpha_P - 1 = \frac{4\alpha_s N_c}{\pi} \ln 2$ is about 30% smaller than the leading-twist contribution to the intercept which yields $(\alpha_P - 1)_{LT} = \frac{4\alpha_s N_c}{\pi}$ (see the discussion on p. 246 of [17]). It is possible that something similar takes place in the helicity evolution case at hand, accounting for the difference between the leading-twist BER calculation [18] and our all-twist intercept (21).

For the flavor nonsinglet helicity evolution we have derived the large-N_c evolution equation (59). The resulting intercept (66) is in compete agreement with BER [19].

To summarize the status of the leading-order calculations of various intercepts mainly resulting from the DLA evolution, in Table I we list the intercepts for flavor singlet and nonsinglet evolution for the unpolarized and helicity-dependent observables. The intercepts for helicity evolution were obtained by us and by BER in various approximations.

It is important to get a better understanding of the numerical importance of these results for the small-x contribution to the quark spin of the proton,

$$S_q(Q^2) = \frac{1}{2}\int_0^1 dx \Delta\Sigma(x, Q^2), \tag{68}$$

with

$$\Delta\Sigma(x, Q^2) = [\Delta u + \Delta\overline{u} + \Delta d + \Delta\overline{d} + \cdots](x, Q^2). \tag{69}$$

A detailed analysis of the impact of our flavor singlet intercept on $\Delta\Sigma(x, Q^2)$ at small x is carried out in [31]. Clearly, large intercepts may potentially lead to a divergent integral in Eq. (68) and would require higher-order corrections or saturation effects at small x to make the integral finite.

To see which of the small-x helicity intercepts give a finite integral in Eq. (68), we compute their numerical values in Table I for $N_c = 3$ and α_s set by the one-loop running coupling expression

$$\alpha_s(Q^2) = \frac{4\pi}{(11 - \frac{2}{3}N_f)\ln\frac{Q^2}{\Lambda^2}} \tag{70}$$

with $\Lambda = 0.192$ GeV and $N_f = 3$ for purposes of the scale-setting. (Since this is a rough estimate, and includes a pure-glue and fixed-N_f numerical estimates of the intercept, we do not change our N_f with Q^2 for simplicity.) For comparison, we have included the leading-order (LO) BFKL intercept [1,2] along with the intercept for the perturbative QCD Reggeon [20–25]. We see that, for a wide range of Q^2, the BER results generate small-x intercepts which are greater than 1 and hence nonintegrable. Our result, on the other hand, generally yields an integrable singularity at $x \to 0$. Indeed this only means that our result would not require higher-order or saturation corrections to give a finite integral in Eq. (68).

Note that a strong 't Hooft coupling calculation [55] in the framework of the anti-de Sitter/conformal field theory (AdS/CFT) correspondence appears to indicate that in $\mathcal{N} = 4$ super–Yang–Mills theory the flavor nonsinglet intercept is smaller than one for all couplings, with the flavor singlet contribution being suppressed at large coupling. If this conclusion applies to QCD, this may indicate that higher-order correction would not allow any of the perturbative intercepts found in this work (α_h or α_h^{NS}) to exceed unity.

TABLE I. Comparison of the intercepts α leading to helicity PDF's which scale as $\Delta q_f(x, Q^2) \propto (\frac{1}{x})^\alpha$ in the high-energy/small-x asymptotics. The LO BFKL Pomeron which sets the small-x asymptotics of unpolarized PDF's is shown for comparison, along with the LO intercept of the perturbative QCD Reggeon. Unless otherwise specified, the quoted intercepts are taken at finite N_c.

Observable	Evolution	Intercept	$Q^2 = 3$ GeV^2 $\alpha_s = 0.343$	$Q^2 = 10$ GeV^2 $\alpha_s = 0.249$	$Q^2 = 87$ GeV^2 $\alpha_s = 0.18$
Unpolarized flavor singlet structure function F_2	LO BFKL Pomeron	$1 + \frac{\alpha_s N_c}{\pi} 4 \ln 2$	1.908	1.659	1.477
Unpolarized flavor nonsinglet structure function F_2	Reggeon	$\sqrt{\frac{2\alpha_s C_F}{\pi}}$	0.540	0.460	0.391
Flavor singlet structure function g_1^S	us (Pure Glue, Large-N_c)	$2.31\sqrt{\frac{\alpha_s N_c}{2\pi}}$	0.936	0.797	0.678
	BER (Pure Glue)	$3.66\sqrt{\frac{\alpha_s N_c}{2\pi}}$	1.481	1.262	1.073
	BER ($N_f = 4$)	$3.45\sqrt{\frac{\alpha_s N_c}{2\pi}}$	1.400	1.190	1.011
Flavor nonsinglet structure function g_1^{NS}	BER and us (Large-N_c)	$\sqrt{\frac{\alpha_s N_c}{\pi}}$	0.572	0.488	0.415

In addition, higher order corrections are needed to obtain a more reliable comparison with the experimental data. Future work on the subject would include solving the flavor singlet evolution equations derived in [29] for the large-N_c & N_f limit, which includes quarks. Another important set of higher-order corrections which should be taken into account in future work is the set of single-logarithmic (LLA) corrections which resum $\alpha_s \ln\frac{1}{x}$. It appears that the light-front formalism used here can be systematically extended to LLA accuracy. Our nonlinear evolution equations already account for one source of LLA corrections: the small-x evolution of the unpolarized dipole $S_{21}(z)$. It is also straightforward to include the LLA corrections analogous to the unpolarized case in which the longitudinal integral generates the logarithm of energy, but the transverse integral does not; these corrections are difficult to include using the method of infrared evolution equations [56]. We are also cautiously optimistic that we can include the LLA corrections with the logarithm of energy arising only from the transverse integral. Including running coupling corrections using the Brodsky–Lepage–Mackenzie (BLM) [57] scheme along the lines of [58–61] for unpolarized evolution (see also [62–64] for other methods used for helicity evolution) would be a natural next step ultimately leading to a detailed comparison to the experimental longitudinal spin data at small x, complementing the existing approaches [56,65–71].

ACKNOWLEDGMENTS

Y. K. is grateful to Boris Ermolaev for a discussion of BER calculation, to Jochen Bartels for correspondence, and to Ian Balitsky for an informative discussion. This material is based upon work supported by the U.S. Department of Energy, Office of Science, Office of Nuclear Physics under Award Number DE-SC0004286 (Y. K.), within the framework of the TMD Topical Collaboration (D. P.), and DOE Contract No. DE-SC0012704 (MS). DP also received support from the RIKEN BNL Research Center. MS received additional support from an EIC program development fund from BNL and from the U.S. Department of Energy, Office of Science under the DOE Early Career Program.

APPENDIX A: TAKING THE LARGE-N_c LIMIT OF HELICITY EVOLUTION

The large-N_c limit means that different dipoles do not "talk" to each other in the process of evolution and interaction with the target. However, when we write a gluon line as a double (quark-antiquark) line, it is a statement only about color factors: this does not mean that all the other dynamical factors associated with the gluon dynamics also split into those for quark and antiquark. Namely, the $G \to GG$ splitting wave function is not, in general, equal to the sum of $q \to qG$ and $\overline{q} \to \overline{q}G$ wave functions. Confusion may arise because in the eikonal limit the $G \to GG$ splitting is, in fact, a sum of $q \to qG$ and $\overline{q} \to \overline{q}G$ wave functions.

To demonstrate this in our case let us start with the evolution equation for the adjoint dipole [Eq. (62) from [29]] keeping flavor-singlet evolution in mind

$$\begin{aligned}\frac{1}{N_c^2-1}\langle\!\langle \mathrm{Tr}[U_{\underline{0}}U_{\underline{1}}^{\mathrm{pol}\dagger}]\rangle\!\rangle(z) &= \frac{1}{N_c^2-1}\langle\!\langle \mathrm{Tr}[U_{\underline{0}}U_{\underline{1}}^{\mathrm{pol}\dagger}]\rangle\!\rangle_0(z) + \frac{\alpha_s}{2\pi^2}\int_{\Lambda^2/s}^{z}\frac{dz'}{z'}\int\frac{d^2x_2}{x_{21}^2}\theta\left(x_{21}^2-\frac{1}{z's}\right)\\ &\times\left\{\theta(x_{10}-x_{21})\frac{4}{N_c^2-1}\langle\!\langle \mathrm{Tr}[T^bU_{\underline{0}}T^aU_{\underline{1}}^\dagger](U_{\underline{2}}^{\mathrm{pol}})^{ba}\rangle\!\rangle(z')\right.\\ &-\theta(x_{10}^2z-x_{21}^2z')\frac{N_f}{N_c^2-1}\langle\!\langle \mathrm{tr}[t^bV_{\underline{1}}t^aV_{\underline{2}}^{\mathrm{pol}\dagger}]U_{\underline{0}}^{ba}+\mathrm{tr}[t^bV_{\underline{2}}^{\mathrm{pol}}t^aV_{\underline{1}}^\dagger]U_{\underline{0}}^{ba}\rangle\!\rangle(z')\\ &\left.+\theta(x_{10}-x_{21})\frac{2}{N_c^2-1}[\langle\!\langle \mathrm{Tr}[T^bU_{\underline{0}}T^aU_{\underline{1}}^{\mathrm{pol}\dagger}]U_{\underline{2}}^{ba}\rangle\!\rangle(z')-N_c\langle\!\langle \mathrm{Tr}[U_{\underline{0}}U_{\underline{1}}^{\mathrm{pol}\dagger}]\rangle\!\rangle(z')]\right\}. \qquad \text{(A1)}\end{aligned}$$

Here the U's are adjoint Wilson lines. Concentrating on the term responsible for the emission of the polarization-carrying soft gluon we write Eq. (A1) as

$$\begin{aligned}\frac{1}{N_c^2-1}\langle\!\langle \mathrm{Tr}[U_{\underline{0}}U_{\underline{1}}^{\mathrm{pol}\dagger}]\rangle\!\rangle(z) &= \frac{1}{N_c^2-1}\langle\!\langle \mathrm{Tr}[U_{\underline{0}}U_{\underline{1}}^{\mathrm{pol}\dagger}]\rangle\!\rangle_0(z) + \frac{\alpha_s}{2\pi}\int_{\frac{1}{x_{10}^2s}}^{z}\frac{dz'}{z'}\int_{\frac{1}{z's}}^{x_{01}^2}\frac{dx_{21}^2}{x_{21}^2}\\ &\times\left\{\frac{4}{N_c^2-1}\langle\!\langle \mathrm{Tr}[T^bU_{\underline{0}}T^aU_{\underline{1}}^\dagger](U_{\underline{2}}^{\mathrm{pol}})^{ba}\rangle\!\rangle(z')+\cdots\right\}. \qquad \text{(A2)}\end{aligned}$$

Our goal here is to properly take the large-N_c limit of (A2), writing the answer in terms of the fundamental dipole operators. To do so we remember that

$$U^{ab} = 2\mathrm{tr}[t^b V^\dagger t^a V], \tag{A3}$$

as expected for Wilson lines.

To write a similar expression for the "polarized adjoint Wilson line" operator, in the large-N_c limit one can think of it as a Wilson line with one insertion of a noneikonal vertex (due to a spin-dependent gluon exchange). Let us model this noneikonal vertex as a (possibly transverse) derivative acting on the true (unpolarized) Wilson line (see e.g. [72]), that is, we write

$$\begin{aligned}(U^{\mathrm{pol}})^{ab} &\propto \partial U^{ab}\\ &= \partial\{2\mathrm{tr}[t^b V^\dagger t^a V]\}\\ &= 2\mathrm{tr}[t^b(\partial V^\dagger)t^a V] + 2\mathrm{tr}[t^b V^\dagger t^a(\partial V)]\\ &\propto 2\mathrm{tr}[t^b V^{\mathrm{pol}\dagger} t^a V] + 2\mathrm{tr}[t^b V^\dagger t^a V^{\mathrm{pol}}].\end{aligned} \tag{A4}$$

In the last step we identified $\partial V \to V^{\mathrm{pol}}$. Using the resulting relation

$$(U^{\mathrm{pol}})^{ab} = 2\mathrm{tr}[t^b V^{\mathrm{pol}\dagger} t^a V] + 2\mathrm{tr}[t^b V^\dagger t^a V^{\mathrm{pol}}] \tag{A5}$$

along with Eq. (A3) to simplify the adjoint polarized dipole operator on the left-hand side of Eq. (A2) we obtain

$$\begin{aligned}&\mathrm{Tr}[U_{\underline{0}} U_{\underline{1}}^{\mathrm{pol}\dagger}]\\ &= U_{\underline{0}}^{ba}(U_{\underline{1}}^{\mathrm{pol}\dagger})^{ab} = U_{\underline{0}}^{ba}(U_{\underline{1}}^{\mathrm{pol}})^{ba}\\ &= 4\mathrm{tr}[t^a V_0^\dagger t^b V_0](\mathrm{tr}[t^a V_1^{\mathrm{pol}\dagger} t^b V_1] + \mathrm{tr}[t^a V_1^\dagger t^b V_1^{\mathrm{pol}}])\\ &= 2\mathrm{tr}[V_0^\dagger t^b V_0 V_1^{\mathrm{pol}\dagger} t^b V_1] + 2\mathrm{tr}[V_0^\dagger t^b V_0 V_1^\dagger t^b V_1^{\mathrm{pol}}]\\ &= \mathrm{tr}[V_0 V_1^{\mathrm{pol}\dagger}]\mathrm{tr}[V_1 V_0^\dagger] + \mathrm{tr}[V_0 V_1^\dagger]\mathrm{tr}[V_1^{\mathrm{pol}} V_0^\dagger] + \cdots,\end{aligned} \tag{A6}$$

where the ellipsis denote the subleading-N_c terms. In arriving at the end result in Eq. (A6) we have applied the Fierz identity twice.

We conclude that

$$\frac{1}{N_c^2-1}\langle\!\langle \mathrm{Tr}[U_{\underline{0}} U_{\underline{1}}^{\mathrm{pol}\dagger}]\rangle\!\rangle(z) = 2G_{10}(z)S_{01}(z) \tag{A7}$$

in the large-N_c limit. Note that the polarized dipole amplitude $G_{10}(z)$ is made out of the quark lines coming from the gluons in the large-N_c limit.

Now let us perform a similar analysis to the operator on the right-hand side of Eq. (A2),

$$\begin{aligned}&\mathrm{Tr}[T^b U_{\underline{0}} T^a U_{\underline{1}}^\dagger](U_{\underline{2}}^{\mathrm{pol}})^{ba}\\ &= -f^{bcd} U_0^{de} f^{aeg}(U_1^\dagger)^{gc} 2\{\mathrm{tr}[t^a V_2^{\mathrm{pol}\dagger} t^b V_2] + \mathrm{tr}[t^a V_2^\dagger t^b V_2^{\mathrm{pol}}]\}\\ &= -8 f^{bcd} f^{aeg}\mathrm{tr}[t^e V_0^\dagger t^d V_0]\mathrm{tr}[t^g V_1^\dagger t^c V_1]\{\mathrm{tr}[t^a V_2^{\mathrm{pol}\dagger} t^b V_2]\\ &\quad + \mathrm{tr}[t^a V_2^\dagger t^b V_2^{\mathrm{pol}}]\}\\ &= 8\mathrm{tr}[t^e V_0^\dagger [t^b, t^c] V_0]\mathrm{tr}[[t^a, t^e] V_1^\dagger t^c V_1]\{\mathrm{tr}[t^a V_2^{\mathrm{pol}\dagger} t^b V_2]\\ &\quad + \mathrm{tr}[t^a V_2^\dagger t^b V_2^{\mathrm{pol}}]\}.\end{aligned} \tag{A8}$$

Let us concentrate on the first two traces: using Fierz identity multiple times we write

$$\begin{aligned}&\mathrm{tr}[t^e V_0^\dagger [t^b, t^c] V_0]\mathrm{tr}[[t^a, t^e] V_1^\dagger t^c V_1]\\ &= \mathrm{tr}[t^e V_0^\dagger (t^b t^c - t^c t^b) V_0]\mathrm{tr}[(t^a t^e - t^e t^a) V_1^\dagger t^c V_1]\\ &= \frac{1}{2}\mathrm{tr}[V_0^\dagger (t^b t^c - t^c t^b) V_0 V_1^\dagger t^c V_1 t^a]\\ &\quad - \frac{1}{2}\mathrm{tr}[V_0^\dagger (t^b t^c - t^c t^b) V_0 t^a V_1^\dagger t^c V_1]\\ &= \frac{1}{4}\mathrm{tr}[V_0 V_1^\dagger]\mathrm{tr}[V_1 t^a V_0^\dagger t^b] - \frac{1}{4}\mathrm{tr}[t^b V_0 V_1^\dagger]\mathrm{tr}[V_1 t^a V_0^\dagger]\\ &\quad - \frac{1}{4}\mathrm{tr}[V_0 t^a V_1^\dagger]\mathrm{tr}[V_1 V_0^\dagger t^b] + \frac{1}{4}\mathrm{tr}[t^b V_0 t^a V_1^\dagger]\mathrm{tr}[V_1 V_0^\dagger].\end{aligned} \tag{A9}$$

Substituting Eq. (A9) into Eq. (A8) and using Fierz identity two more times we arrive at

$$\begin{aligned}&\mathrm{Tr}[T^b U_{\underline{0}} T^a U_{\underline{1}}^\dagger](U_{\underline{2}}^{\mathrm{pol}})^{ba}\\ &= 2\{\mathrm{tr}[t^a V_2^{\mathrm{pol}\dagger} t^b V_2] + \mathrm{tr}[t^a V_2^\dagger t^b V_2^{\mathrm{pol}}]\}\\ &\quad \times \{\mathrm{tr}[V_0 V_1^\dagger]\mathrm{tr}[V_1 t^a V_0^\dagger t^b] - \mathrm{tr}[t^b V_0 V_1^\dagger]\mathrm{tr}[V_1 t^a V_0^\dagger]\\ &\quad - \mathrm{tr}[V_0 t^a V_1^\dagger]\mathrm{tr}[V_1 V_0^\dagger t^b] + \mathrm{tr}[t^b V_0 t^a V_1^\dagger]\mathrm{tr}[V_1 V_0^\dagger]\}\\ &= \frac{1}{2}\mathrm{tr}[V_0 V_1^\dagger]\mathrm{tr}[V_2^{\mathrm{pol}} V_0^\dagger]\mathrm{tr}[V_1 V_2^\dagger]\\ &\quad + \frac{1}{2}\mathrm{tr}[V_0 V_1^\dagger]\mathrm{tr}[V_2 V_0^\dagger]\mathrm{tr}[V_1 V_2^{\mathrm{pol}\dagger}]\\ &\quad + \frac{1}{2}\mathrm{tr}[V_0 V_1^\dagger]\mathrm{tr}[V_2^{\mathrm{pol}} V_1^\dagger]\mathrm{tr}[V_0 V_2^\dagger]\\ &\quad + \frac{1}{2}\mathrm{tr}[V_0 V_1^\dagger]\mathrm{tr}[V_2 V_1^\dagger]\mathrm{tr}[V_0 V_2^{\mathrm{pol}\dagger}] + \cdots,\end{aligned} \tag{A10}$$

where the ellipsis denote the N_c-suppressed term, which include operators which are N_c-suppressed due to consisting of fewer than three traces but not suppressed by explicit factors of $1/N_c$.

We thus conclude that in the large-N_c limit

$$\frac{1}{N_c^2-1}\langle\!\langle \mathrm{Tr}[T^b U_{\underline{0}} T^a U_{\underline{1}}^\dagger](U_{\underline{2}}^{\mathrm{pol}})^{ba}\rangle\!\rangle(z) = N_c S_{01}(z)[S_{02}(z)G_{21}(z) + S_{21}(z)\Gamma_{02,21}(z)]. \quad \text{(A11)}$$

Substituting Eqs. (A7) and (A11) into Eq. (A2) we arrive at

$$G_{10}(z) = G_{10}^{(0)}(z) + \frac{\alpha_s N_c}{2\pi}\int_{\frac{1}{x_{10}^2 s}}^{z}\frac{dz'}{z'}\int_{\frac{1}{z's}}^{x_{01}^2}\frac{dx_{21}^2}{x_{21}^2} \times [2S_{02}(z')G_{21}(z') + 2S_{21}(z')\Gamma_{02,21}(z') + \cdots], \quad \text{(A12)}$$

in agreement with the first two terms in the integral on the right of Eqs. (16).

Note that in arriving at Eq. (A12) we have implicitly assumed that

$$\frac{1}{N_c^2-1}\langle\!\langle \mathrm{Tr}[U_{\underline{0}} U_{\underline{1}}^{\mathrm{pol}\dagger}]\rangle\!\rangle_0(z) = 2G_{10}^{(0)}(z)S_{01}(z) \quad \text{(A13)}$$

with a fully (LLA) evolved $S_{01}(z)$. Hence Eq. (A12) can be thought of as helicity evolution in the background of the unpolarized LLA evolution.

APPENDIX B: REPRODUCING BER

In order to establish a connection between our work and the paper by BER [18] we tried calculating the first small-x evolution correction to the Born-level cross section mediated by the gluon exchanges. We performed our calculation in the Feynman gauge, just like the authors of [18] did. (Note that our evolution calculations here and in [29] were done in the light cone gauge.) The diagrams we analyzed are shown in Fig. 12, where we concentrate on real gluon emissions only. As usual in high-energy scattering we work in the eikonal limit where

$$p_1^+, p_2^- \gg k_1^+, k_2^-, k_{1\perp}, k_{2\perp} \gg k_1^-, k_2^+. \quad \text{(B1)}$$

For simplicity we put $p_1^- = 0 = p_2^+$ and $\underline{p}_1 = 0 = \underline{p}_2$.

We are interested in the parts of the diagrams contributing to the double-spin asymmetry. Keeping the $\sigma_1\sigma_2$ terms only and performing a direct calculation we obtain the following leading in energy contributions to the amplitude squared:

$$\langle|M|^2\rangle|_A = 16g^6 C_F\sigma_1\sigma_2\frac{s}{k_{1\perp}^2 k_{2\perp}^2}, \quad \text{(B2a)}$$

$$\langle|M|^2\rangle|_B = 4g^6 C_F\sigma_1\sigma_2 s\frac{\underline{k}_2\cdot(\underline{k}_1-2\underline{k}_2)}{k_{1\perp}^2 k_{2\perp}^4} \approx -8g^6 C_F\sigma_1\sigma_2\frac{s}{k_{1\perp}^2 k_{2\perp}^2}, \quad \text{(B2b)}$$

$$\langle|M|^2\rangle|_C = 4g^6 C_F\sigma_1\sigma_2 s\frac{\underline{k}_2\cdot(\underline{k}_1-2\underline{k}_2)}{k_{1\perp}^2 k_{2\perp}^4} \approx -8g^6 C_F\sigma_1\sigma_2\frac{s}{k_{1\perp}^2 k_{2\perp}^2}, \quad \text{(B2c)}$$

$$\langle|M|^2\rangle|_D = 4g^6\frac{C_F}{N_c^2}\sigma_1\sigma_2 s\frac{k_{1\perp}^2+k_{2\perp}^2+(\underline{k}_1-\underline{k}_2)^2}{k_{1\perp}^2 k_{2\perp}^2(\underline{k}_1-\underline{k}_2)^2}, \quad \text{(B2d)}$$

$$\langle|M|^2\rangle|_E = 4g^6\frac{C_F(N_c^2-2)}{N_c^2}\sigma_1\sigma_2 s\frac{k_{1\perp}^2+k_{2\perp}^2+(\underline{k}_1-\underline{k}_2)^2}{k_{1\perp}^2 k_{2\perp}^2(\underline{k}_1-\underline{k}_2)^2}, \quad \text{(B2e)}$$

$$\langle|M|^2\rangle|_F = 0, \quad \text{(B2f)}$$

$$\langle|M|^2\rangle|_G = 0, \quad \text{(B2g)}$$

$$\langle|M|^2\rangle|_H = 0, \quad \text{(B2h)}$$

$$\langle|M|^2\rangle|_I = 4g^6\frac{C_F}{N_c^2}\sigma_1\sigma_2 s\frac{k_{1\perp}^2+k_{2\perp}^2+(\underline{k}_1-\underline{k}_2)^2}{k_{1\perp}^2 k_{2\perp}^2(\underline{k}_1-\underline{k}_2)^2}. \quad \text{(B2i)}$$

Note that in arriving at Eqs. (B2) we have added the top-down and left-right mirror images of diagrams B, C, E, H, and the up-down mirror images of D, F, G, I, as these transformations generate new diagrams. The approximate expressions for diagrams B and C are obtained by keeping their DLA contributions only: in such contributions, the integration over the angles of $\underline{k}_1$ and/or $\underline{k}_2$ eliminates the first term in the initial expressions for B and C. Note that, after the extraction of these DLA contribution, diagrams B and C cancel the diagram A,

$$\langle|M|^2\rangle|_A + \langle|M|^2\rangle|_B + \langle|M|^2\rangle|_C = 0. \quad \text{(B3)}$$

This is in complete analogy with the unpolarized (BFKL) case. Namely, if we keep the leading-energy polarization-independent contributions of the diagrams in Fig. 12, then Eq. (B3) would still hold.

The sum of all the diagrams in Fig. 12 is then given by the contributions of the bremsstrahlung diagrams D—I. We get

$$\langle|M|^2\rangle|_A + \langle|M|^2\rangle|_B + \cdots + \langle|M|^2\rangle|_I = 4g^6 C_F\sigma_1\sigma_2 s\frac{k_{1\perp}^2+k_{2\perp}^2+(\underline{k}_1-\underline{k}_2)^2}{k_{1\perp}^2 k_{2\perp}^2(\underline{k}_1-\underline{k}_2)^2}. \quad \text{(B4)}$$

At this point it is appropriate to compare these results with the discussion of Fig. 7 in [18]. Our diagrams B and C from Fig. 12 can be identified with the diagrams (d) and (c) in Fig. 7 of [18], respectively, if one discards the virtual photon lines and the upper quark propagator in the latter. The discussion following Eq. (2.32) and continuing until the end of Sec. II in [18] also notes that Eq. (B3) holds for

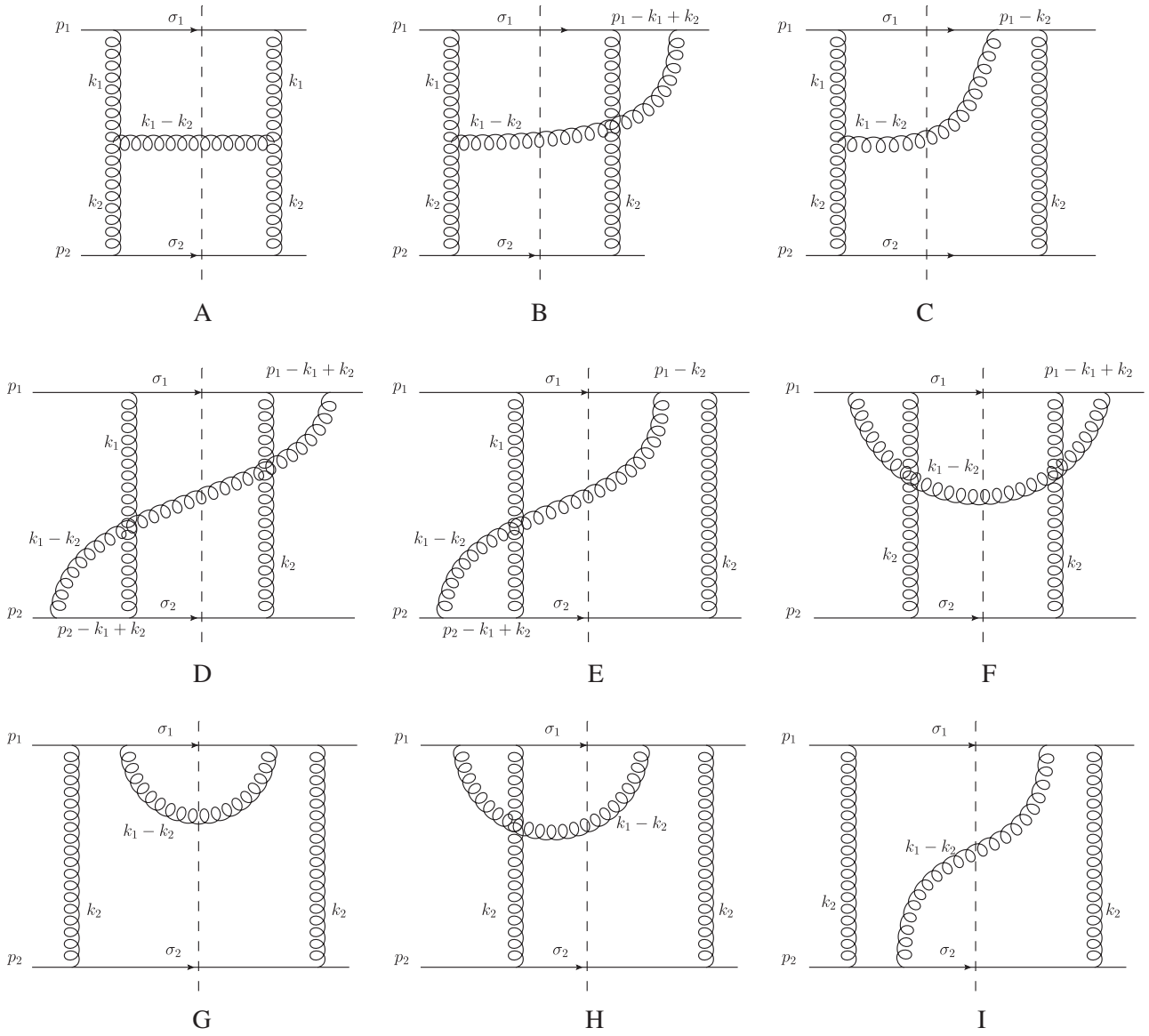

FIG. 12. Diagrams representing one-loop DLA helicity evolution corrections to the Born-level graphs in Feynman gauge. Dashed lines denote the final state cuts. Only corrections with the extra gluon going through the final state cut are considered.

the BFKL case, but appears to suggest that for helicity evolution Eq. (B3) does not hold, and, instead, one has

$$\langle |M|^2 \rangle|_B + \langle |M|^2 \rangle|_C \overset{\text{BER}}{=} 0. \tag{B5}$$

The conclusion (B5) was reached in [18] for the contribution of graphs B and C coming from the $k' = |\underline{k}_1 - \underline{k}_2| \gg k_1$ regime, which seems to be identical to $k_2 \gg k_1$ region of phase space, in which diagrams B and C are DLA. Guided by Eq. (B5), the authors of [18] conclude that diagrams B and C cancel in the $k_2 \gg k_1$ regime, and need to be considered in the $k' = |\underline{k}_1 - \underline{k}_2| \ll k_1, k_2$ region only, where Gribov's theorem [73] applies.

The conclusion (B5) reached in [18] seems to contradict the results of a direct calculation presented above in Eqs. (B2) and resulting in Eq. (B3). Note that our diagrams B and C come in with the same overall sign: this is due to their color factors being different by a minus sign along with another minus sign coming from the difference between the quark propagators to the right of the cut. If Eq. (B5) is incorrect, it appears the infrared evolution equations (IREE) derived in [18] would need to be modified, though we do not quite see how they could be changed to easily accommodate the contributions of non-ladder graphs B and C in the $k_2 \gg k_1$ regime, where Gribov's theorem does not apply. Note also that diagrams D, E and I give DLA contributions in the same $k_2 \gg k_1$ regime, which do not cancel the contributions of B and C from the same region of the phase space: it appears that such contributions of D, E and I were not discussed in [18],

and they seem not to be taken into account by the resulting IREE.

It is also possible that we misunderstood the discussion in [18] and the conclusion there was not given by Eq. (B5), but, rather, the conclusion was that each diagram B and C separately is not DLA in the $k_2 \gg k_1$ regime. Unfortunately this also seems to contradict the results of our calculations above in Eqs. (B2), which show that the contributions of diagrams B and C have the same momentum dependence as that of diagram A, and hence B and C are DLA in the $k_2 \gg k_1$ regime in question, since A is also DLA in this region.

[1] E. A. Kuraev, L. N. Lipatov, and V. S. Fadin, The Pomeranchuk singlularity in non-Abelian gauge theories, Sov. Phys. JETP **45**, 199 (1977).

[2] I. Balitsky and L. Lipatov, The Pomeranchuk singularity in quantum chromodynamics, Sov. J. Nucl. Phys. **28**, 822 (1978).

[3] I. Balitsky, Operator expansion for high-energy scattering, Nucl. Phys. **B463**, 99 (1996).

[4] I. Balitsky, Factorization and high-energy effective action, Phys. Rev. D **60**, 014020 (1999).

[5] Y. V. Kovchegov, Small-x F_2 structure function of a nucleus including multiple pomeron exchanges, Phys. Rev. D **60**, 034008 (1999).

[6] Y. V. Kovchegov, Unitarization of the BFKL pomeron on a nucleus, Phys. Rev. D **61**, 074018 (2000).

[7] J. Jalilian-Marian, A. Kovner, and H. Weigert, The Wilson renormalization group for low x physics: Gluon evolution at finite parton density, Phys. Rev. D **59**, 014015 (1998).

[8] J. Jalilian-Marian, A. Kovner, A. Leonidov, and H. Weigert, The Wilson renormalization group for low x physics: Towards the high density regime, Phys. Rev. D **59**, 014014 (1998).

[9] E. Iancu, A. Leonidov, and L. D. McLerran, The renormalization group equation for the color glass condensate, Phys. Lett. B **510**, 133 (2001).

[10] E. Iancu, A. Leonidov, and L. D. McLerran, Nonlinear gluon evolution in the color glass condensate. I, Nucl. Phys. **A692**, 583 (2001).

[11] L. V. Gribov, E. M. Levin, and M. G. Ryskin, Semihard processes in QCD, Phys. Rep. **100**, 1 (1983).

[12] E. Iancu and R. Venugopalan, The color glass condensate and high energy scattering in QCD, Quark-Gluon Plasma **3**, 249 (2004).

[13] H. Weigert, Evolution at small x_{bj}: The color glass condensate, Prog. Part. Nucl. Phys. **55**, 461 (2005).

[14] J. Jalilian-Marian and Y. V. Kovchegov, Saturation physics and deuteron gold collisions at RHIC, Prog. Part. Nucl. Phys. **56**, 104 (2006).

[15] F. Gelis, E. Iancu, J. Jalilian-Marian, and R. Venugopalan, The color glass condensate, Annu. Rev. Nucl. Part. Sci. **60**, 463 (2010).

[16] J. L. Albacete and C. Marquet, Gluon saturation and initial conditions for relativistic heavy ion collisions, Prog. Part. Nucl. Phys. **76**, 1 (2014).

[17] Y. V. Kovchegov and E. Levin, *Quantum Chromodynamics at High Energy* (Cambridge University Press, Cambridge, England, 2012).

[18] J. Bartels, B. I. Ermolaev, and M. G. Ryskin, Flavor singlet contribution to the structure function G(1) at small x, Z. Phys. C **72**, 627 (1996).

[19] J. Bartels, B. Ermolaev, and M. Ryskin, Nonsinglet contributions to the structure function g1 at small x, Z. Phys. C **70**, 273 (1996).

[20] R. Kirschner and L. Lipatov, Double logarithmic asymptotics and Regge singularities of quark Amplitudes with flavor exchange, Nucl. Phys. **B213**, 122 (1983).

[21] R. Kirschner, Regge asymptotics of scattering amplitudes in the logarithmic approximation of QCD, Z. Phys. C **31**, 135 (1986).

[22] R. Kirschner, Regge asymptotics of scattering with flavor exchange in QCD, Z. Phys. C **67**, 459 (1995).

[23] R. Kirschner, Reggeon interactions in perturbative QCD, Z. Phys. C **65**, 505 (1995).

[24] S. Griffiths and D. Ross, Studying the perturbative Reggeon, Eur. Phys. J. C **12**, 277 (2000).

[25] K. Itakura, Y. V. Kovchegov, L. McLerran, and D. Teaney, Baryon stopping and valence quark distribution at small x, Nucl. Phys. **A730**, 160 (2004).

[26] Y. L. Dokshitzer, Calculation of the structure functions for deep inelastic scattering and e^+e^- annihilation by perturbation theory in quantum chromodynamics, Sov. Phys. JETP **46**, 641 (1977).

[27] V. N. Gribov and L. N. Lipatov, Deep inelastic e p scattering, Sov. J. Nucl. Phys. **15**, 438 (1972).

[28] G. Altarelli and G. Parisi, Asymptotic freedom in parton language, Nucl. Phys. **B126**, 298 (1977).

[29] Y. V. Kovchegov, D. Pitonyak, and M. D. Sievert, Helicity evolution at small x, J. High Energy Phys. 01 (2016) 072.

[30] G. P. Lepage and S. J. Brodsky, Exclusive processes in perturbative quantum chromodynamics, Phys. Rev. D **22**, 2157 (1980).

[31] Y. V. Kovchegov, D. Pitonyak, and M. D. Sievert, Small-x asymptotics of the quark helicity distribution, Phys. Rev. Lett. **118**, 052001 (2017).

[32] R. Mertig and W. L. van Neerven, The calculation of the two loop spin splitting functions P(ij)(1)(x), Z. Phys. C **70**, 637 (1996).

[33] Y. V. Kovchegov and M. D. Sievert, Calculating TMDs of an unpolarized target: Quasi-classical approximation and quantum evolution, Nucl. Phys. **B903**, 164 (2016).

[34] J. Bjorken, J. B. Kogut, and D. E. Soper, Quantum electrodynamics at infinite momentum: Scattering from an external field, Phys. Rev. D **3**, 1382 (1971).

[35] N. N. Nikolaev and B. G. Zakharov, Colour transparency and scaling properties of nuclear shadowing in deep inelastic scattering, Z. Phys. C **49**, 607 (1991).
[36] Y. Hatta, E. Iancu, K. Itakura, and L. McLerran, Odderon in the color glass condensate, Nucl. Phys. **A760**, 172 (2005).
[37] Y. V. Kovchegov, L. Szymanowski, and S. Wallon, Perturbative odderon in the dipole model, Phys. Lett. B **586**, 267 (2004).
[38] A. H. Mueller, Small x behavior and parton saturation: A QCD model, Nucl. Phys. **B335**, 115 (1990).
[39] L. D. McLerran and R. Venugopalan, Computing quark and gluon distribution functions for very large nuclei, Phys. Rev. D **49**, 2233 (1994).
[40] L. D. McLerran and R. Venugopalan, Gluon distribution functions for very large nuclei at small transverse momentum, Phys. Rev. D **49**, 3352 (1994).
[41] L. D. McLerran and R. Venugopalan, Green's functions in the color field of a large nucleus, Phys. Rev. D **50**, 2225 (1994).
[42] Y. V. Kovchegov, Non-Abelian Weizsaecker-Williams field and a two- dimensional effective color charge density for a very large nucleus, Phys. Rev. D **54**, 5463 (1996).
[43] Y. V. Kovchegov, Quantum structure of the non-Abelian Weizsaecker-Williams field for a very large nucleus, Phys. Rev. D **55**, 5445 (1997).
[44] J. Jalilian-Marian, A. Kovner, L. D. McLerran, and H. Weigert, The intrinsic glue distribution at very small x, Phys. Rev. D **55**, 5414 (1997).
[45] H. Weigert, Unitarity at small Bjorken x, Nucl. Phys. **A703**, 823 (2002).
[46] A. H. Mueller, Soft gluons in the infinite momentum wave function and the BFKL pomeron, Nucl. Phys. **B415**, 373 (1994).
[47] A. H. Mueller and B. Patel, Single and double BFKL pomeron exchange and a dipole picture of high-energy hard processes, Nucl. Phys. **B425**, 471 (1994).
[48] A. H. Mueller, Unitarity and the BFKL pomeron, Nucl. Phys. **B437**, 107 (1995).
[49] L. D. McLerran and R. Venugopalan, Fock space distributions, structure functions, higher twists and small x, Phys. Rev. D **59**, 094002 (1999).
[50] S. J. Brodsky, H.-C. Pauli, and S. S. Pinsky, Quantum chromodynamics and other field theories on the light cone, Phys. Rep. **301**, 299 (1998).
[51] G. A. Chirilli, Y. V. Kovchegov, and D. E. Wertepny, Classical gluon production amplitude for nucleus-nucleus collisions: First saturation correction in the projectile, J. High Energy Phys. 03 (**2015**) 015.
[52] J. Blumlein and A. Vogt, The singlet contribution to the structure function g1 (x, Q^2) at small x, Phys. Lett. B **386**, 350 (1996).
[53] S. Moch, J. A. M. Vermaseren, and A. Vogt, The three-loop splitting functions in QCD: The helicity-dependent case, Nucl. Phys. **B889**, 351 (2014).
[54] Z. Chen and A. H. Mueller, The dipole picture of high-energy scattering, the BFKL equation and many gluon compound states, Nucl. Phys. **B451**, 579 (1995).
[55] Y. Hatta, T. Ueda, and B.-W. Xiao, Polarized DIS in $N = 4$ SYM: Where is spin at strong coupling?, J. High Energy Phys. 08 (2009) 007.
[56] B. I. Ermolaev, M. Greco, and S. I. Troyan, Overview of the spin structure function g(1) at arbitrary x and Q^2, Riv. Nuovo Cimento Soc. Ital. Fis. **33**, 57 (2010).
[57] S. J. Brodsky, G. P. Lepage, and P. B. Mackenzie, On the elimination of scale ambiguities in perturbative quantum chromodynamics, Phys. Rev. D **28**, 228 (1983).
[58] I. I. Balitsky, Quark contribution to the small-x evolution of color dipole, Phys. Rev. D **75**, 014001 (2007).
[59] J. Kuokkanen, K. Rummukainen, and H. Weigert, HERA-data in the light of small x evolution with state of the art NLO input, Nucl. Phys. **A875**, 29 (2012).
[60] Y. Kovchegov and H. Weigert, Triumvirate of Running Couplings in Small-x Evolution, Nucl. Phys. **A784**, 188 (2007).
[61] Y. V. Kovchegov and H. Weigert, Quark loop contribution to BFKL evolution: Running coupling and leading-N(f) NLO intercept, Nucl. Phys. **A789**, 260 (2007).
[62] B. I. Ermolaev, M. Greco, and S. I. Troian, QCD running coupling effects for the nonsinglet structure function at small x, Nucl. Phys. **B571**, 137 (2000).
[63] B. I. Ermolaev, M. Greco, and S. I. Troyan, Intercepts of the nonsinglet structure functions, Nucl. Phys. **B594**, 71 (2001).
[64] B. I. Ermolaev, M. Greco, and S. I. Troyan, Running coupling effects for the singlet structure function g(1) at small x, Phys. Lett. B **579**, 321 (2004).
[65] J. Soffer and O. V. Teryaev, Neutron spin dependent structure function, Bjorken sum rule, and first evidence for singlet contribution at low x, Phys. Rev. D **56**, 1549 (1997).
[66] Y. Kiyo, J. Kodaira, and H. Tochimura, Does leading ln x resummation predict the rise of g(1) at small x?, Z. Phys. C **74**, 631 (1997).
[67] J. Blumlein and A. Vogt, On the behavior of nonsinglet structure functions at small x, Phys. Lett. B **370**, 149 (1996).
[68] J. Blumlein and H. Bottcher, QCD analysis of polarized deep inelastic data and parton distributions, Nucl. Phys. **B636**, 225 (2002).
[69] D. de Florian, R. Sassot, M. Stratmann, and W. Vogelsang, Extraction of spin-dependent parton densities and their uncertainties, Phys. Rev. D **80**, 034030 (2009).
[70] D. de Florian, R. Sassot, M. Stratmann, and W. Vogelsang, Evidence for Polarization of Gluons in the Proton, Phys. Rev. Lett. **113**, 012001 (2014).
[71] E. C. Aschenauer, R. Sassot, and M. Stratmann, Unveiling the proton spin decomposition at a future electron-ion collider, Phys. Rev. D **92**, 094030 (2015).
[72] T. Altinoluk, N. Armesto, G. Beuf, M. Martínez, and C. A. Salgado, Next-to-eikonal corrections in the CGC: Gluon production and spin asymmetries in pA collisions, J. High Energy Phys. 07 (2014) 068.
[73] V. N. Gribov, Yad. Fiz. **5**, 399 (1967) [Bremsstrahlung of hadrons at high energies, Sov. J. Nucl. Phys. **5**, 280 (1967)].